arXiv:astro-ph/0405051v1 4 May 2004

The Kast Ground Based UV Spectral Survey of 79 QSOs at Redshift 2 for Lyman Alpha Forest and Metal Absorption

David Tytler[1,2], John M. O'Meara[1], Nao Suzuki[1], David Kirkman[1], Dan Lubin[1], and Adam Orin[1]

ABSTRACT

We present a moderate resolution ($\sim$ 1.15 Å/pixel) survey of 79 quasars obtained using the Kast spectrograph on the Shane 3m telescope at Lick observatory. The spectra span the wavelength range of 3175–5880 Å, and have typical signal to noise of 6–20 in the regions of the spectra showing Lyα forest absorption. The quasars have a mean emission redshift of $z_{\rm em}$= 2.17, and nearly all cover the entire Lyα forest between Lyα and Lyβ. Although the quasars were selected to avoid BAL, two quasars in the survey are BAL, one of which is a new discovery. We list the H I and metal ions observed in a total of 140 absorption systems. We also identify 526 emission lines, and list their observed wavelengths, along with new redshifts of the quasars. We determine the rest wavelengths of 3 emission lines or line blends in the forest to be 1070.95 ± 1.00, 1123.13 ± 0.51, and 1175.88 ± 0.30 Å.

Subject headings: quasars: absorption lines – quasars: emission lines – cosmology: observations

1. Introduction

In recent years, the ability to obtain precision cosmological measurements from the high redshift intergalactic medium (IGM) has been realized via the combination of large datasets and numerical simulations. Large QSO surveys such as the Sloan Digital Sky Survey (SDSS[1]) and the Two Degree Field Survey (2dF[2]) have made available spectra of thousands of quasars sampling the universe in Lyα forest absorption at redshifts $z \simeq 2.5$ and larger.

---

[1] Center for Astrophysics and Space Sciences, University of California, San Diego, MS 0424; La Jolla; CA 92093-0424

[2] E-Mail: tytler@ucsd.edu

[1] http://www.sdss.org

[2] http://www.aao.gov.au/2df/

At redshifts below 2.5, however, few moderately sized ground based surveys exist which cover the Lyα forest with sufficient resolution or signal to noise. Kim et al (2004) discuss the Lyα forest from a sample of 27 high resolution VLT/UVES spectra with a median redshift of $\langle z \rangle = 2.25$. Scott, Bechtold, and Dobrzycki (2000) present ~ 1Å resolution data for 39 QSOs targeted specifically to cover the Lyα forest at $1.6 < z < 2$. The survey of Lyman limit absorption by Sargent, Steidel, and Boksenberg (1989) contains 59 QSOs, some of which covering the Lyα forest at $z < 2.5$, but the resolution is low, and the bulk of the data is at higher redshift. Barthel, Tytler, and Thompson (1990) present 67 spectra of radio loud quasars, of which 26 have emission redshifts between 1.9 and 2.6, but this survey contains no data below 3880 Å. Sargent, Boksenberg, and Steidel (1988) discuss ~ 1.5Å resolution spectra of 55 QSOs, of which 33 have emission redshifts between 1.9 and 2.5, but this survey was targeted entirely for C IV absorption, and covered only wavelengths suitable for this metal transition. Lanzetta, Wolfe, and Turnshek (1987) analyze 32 quasars for Mg II absorption, 16 of which have emission redshifts between 1.9 and 2.5, but their survey was constrained to wavelengths greater than 6200 Å, and thus does not cover the Lyα forest. Finally, larger surveys such as the Large Bright Quasar Survey (Hewett, Foltz, and Chaffee, 1995), the FIRST Bright QSO Survey (Gregg et al, 1996) and the Hamburg/ESO survey for bright QSOs (Wisotzki et al., 2000) have a large number of QSOs below $z = 2.5$, but the resolution of these surveys is very low.

The scarcity of ground based data covering the Lyα forest at redshifts 1.6–2.5 occurs primarily because working at observed wavelengths less than 4000 Å becomes prohibitive due to issues such as poor fiber optic transmission, diminishing CCD response, and increased effects of atmospheric extinction.

In this paper, we present a survey of 79 quasars with an average emission redshift of $z_{\rm em}= 2.17$. The redshift range of the Lyα forest in the survey serves as a compliment to larger surveys at higher redshift, and is of sufficient size to provide a statistically useful sampling of the IGM at a redshift of 2. Various details of the survey are also discussed in Tytler et al. (2004), where we present a measurement and interpretation of the mean amount of absorption due to H I in the $z \sim 2$ intergalactic medium.

In section 2, we detail the observations and data reduction. In section 3, we present the spectra, and discuss individual quasars, metal absorption systems, and emission lines.

2. Observations and Data Reduction

The data in the survey were obtained using the Kast double spectrograph on the Shane 3m telescope at Lick observatory over the years 2001 through 2003. In most cases, the spectra were obtained using the 2 arcsecond slit width, although some observations required the 3 arcsecond slit to accommodate poor seeing conditions, and in very rare cases, a 1.5 arcsecond slit was used when the seeing conditions were very good. In all observations, the spectrograph slit was oriented such that it was aligned with the vertical direction at the effective middle of the exposure to minimize losses due to atmospheric dispersion. For each QSO in the sample, exposures were taken using both the blue and red cameras on Kast. The blue camera used the 830/4360 grism, and the red camera used the 1200/5000 grating, with a dispersion of 1.13 and 1.17 Å per pixel respectively ($\sim$ 3 pixels per resolution element). We employed the d46 dichroic to split the light between the cameras. The blue camera exposures covered the approximate wavelength range of 3175–4540 Å, and the red camera exposures covered the approximate wavelength range 4475–5880 Å. Because of differences in the exact location of the blue camera CCD on a given observing run, the starting and ending wavelengths varied by approximately ± 5 Å.

The quasars in the survey were all chosen from the NED extragalactic database [3] with only the constraints that they have an emission redshift between $z_{\rm em}$= 1.9 and $z_{\rm em}$= 2.4, be of sufficient brightness to keep exposure times less than a few hours, and not show BAL absorption. The $z_{\rm em}$ constraint was made so as to maximize coverage of the Lyα forest at $z \simeq 1.9$, and the choice to neglect BAL QSOs was made to minimize contaminating absorption in the spectra that do not come from the IGM. We obtained and present spectra for two QSOs, Q1542+5408 and Q2310+0018, which we found to show BAL absorption. Q1542+5408 is discussed in Green et al. (2001), and Q2310+0018 is discovered to be BAL in this survey. Other than these constraints, the survey is unbiased with respect to the quasars observed.

Table 1 lists the QSOs observed, along with their B1950 and J2000 coordinates, the V magnitude as given by NED, the approximate redshift, and the exposure time. For simplicity, and to aid comparison with published spectra, we choose to name the QSOs by their abbreviated B1950 coordinates. Table 2 lists the observation date, slit width and signal to noise for each QSO. The signal to noise in table is calculated at two rest wavelengths, 1070Å and 1170Å and is given as the mean signal to noise over 20 Å centered about these wavelengths. It should be noted that the true signal to noise of the spectrum will be in general higher, because absorption from the Lyα forest lowers the mean signal to noise.

---

[3] http://nedwww.ipac.caltech.edu

These wavelengths were chosen because they correspond to the starting and ending rest wavelengths that were used to sample the Lyα forest for the measurement of the mean flux decrement in Tytler et al. (2004). Figure 1 shows the distribution in signal to noise corresponding to the values in Table 2.

The exposure times were chosen with the intent to obtain S/N > 10.0 at wavelengths greater than the Lyβ emission line of each QSO In practice, most of the spectra reach this goal, except those observed in poor conditions. We do not present QSOs for which we obtained S/N < 2.

We obtained, but do not present spectra for 6 objects which upon reduction, are not QSOs. Two of these spectra are likely due to telescope pointing error. It is possible that the 4 other objects, Q1456+5404 (14h56m47.71 +54d04m25.6 $z_{\rm em}$= 2.300 V=16.50), Q1742+3749 (17h42m 5.55 +37d49m08.3 $z_{\rm em}$= 1.958 V=16.40), Q1755+5749 (17h55m15.97 +57d49m06.9 $z_{\rm em}$= 2.110 V=18.00), and Q2113+3004 (21h13m59.42 +30d04m02.4 $z_{\rm em}$= 2.080 V=17.30) are not QSOs.

All QSOs were reduced using the standard longslit reduction tools in IRAF. Wavelength calibration was also performed in the standard manner with IRAF. For each QSO, an arclamp observation was made at the same telescope position as that for the QSO to minimize the effects that flexure may have on the wavelength solution, and typical wavelength errors were less than 1 Å. For each night, a number of spectrophotometric flux standard stars were observed for the purposes of flux calibration. We list these stars in Table 3. As discussed in Suzuki et al. (2003), our errors in relative flux calibration could be as good as a few percent. Finally, the spectra were cleaned of any deviant pixels resulting from poor sky or cosmic ray subtraction by replacing these pixels with their neighboring flux values.

For the blue camera exposures, a continuum level was placed on the spectrum by eye using the b-spline continuum fitting procedure discussed in Kirkman et.al (2003) and Tytler et. al (2004). On average, in the regions containing Lyα forest absorption, the errors in this continuum level placement were $< 5\%$. A thorough discussion of the continuum level error is given in Tytler et. al (2004). The red camera exposures had no continuum level assigned.

3. The Kast $z \simeq 2$ Survey

We now present the spectra of the survey, comment on absorbers in individual QSOs, and tabulate the emission lines.

3.1. Spectra

In Figures 2–21, we show the blue and red camera exposures of the 79 quasars which comprise the survey. For each blue exposure, the flux (solid line), error (dotted line), and continuum (dashed line) level is shown. For the red camera exposures, we display the flux and error levels. The spectra have well calibrated relative flux, but we do not assign a numerical value to the flux, since absolute flux calibration was not a goal for the survey, and few exposures were made under photometric conditions.

3.2. Notes on Individual QSO Spectra

We now discuss various aspects of the individual QSO spectra in the survey. Table 4 lists 140 systems with strong absorption in H I and metals. These systems were found by scanning the blue camera spectra by eye to find systems which showed Lyα absorption which appeared to have either significant equivalent width, saturated absorption, or a combination of the two. For those systems, both the blue and red camera exposures were then scanned for metal absorption at the same redshift as the H I absorber. Finally, both blue and red camera exposures were inspected for strong metal absorption. When absorption was found, the ion was identified, and the spectra were scanned for absorption from other metal species at that redshift. Spectral regions containing Lyα forest absorption were not scanned for metal lines, as they would be blended with H I, and possibly misidentified. In some cases, only a metal transition such as C IV, Mg II, or Fe II is given, since the H I at the redshift of these absorbers is either outside of the spectral coverage of the data, or is not visually strong compared to the local Lyα forest at nearby wavelengths.

Table 4 is not a complete census of the metal absorption for the survey, but instead attempts to highlight systems with a large H I column density, such as Lyman limit and damped Lyman alpha systems, along with systems showing strong absorption in metals. Additional notes on individual QSOs are given below.

Q1422+4224: There appears to be strong H I absorption at $z = 1.951$. Possible absorption in metals at the expected positions of C II and Si IV is seen, but the SNR at these wavelengths is poor.

Q1542+3104: This QSOs contains considerable metal absorption near the C IV emission line. Moreover, the Lyα forest in this QSOs appears to have many regions of highly clustered absorption. This QSO could be interpreted as a BAL (Weymann et al., 1991; Narayanan et al., 2004).

Q1559+0853: The absorption from C II corresponding at $z = 2.252$ is uncertain, since the Si II absorption from the system at $z = 1.842$ places Si II at nearly the same wavelengths.

Q1649+4007: The Fe II transitions for the absorber at $z = 0.499$ which shows Mg II are all in the Lyα forest, and are thus uncertain.

3.3. Emission Lines

Large samples of quasar emission line wavelengths have been presented and discussed by many authors (Wills, Netzer and Wills, 1985; Weymann et al., 1991; Tytler and Fan, 1992; Laor et al. 1995; Forster et al. 2001; Constantin et al., 2002 and many others). For this survey, we also present the observed emission line wavelengths.

For each quasar in the survey, we attempted to identify all emission lines with wavelengths greater than the O VI–Lyβ emission line blend. The results of the emission line identifications are given in Table 5, where the observed wavelengths for each emission line are given. In total, 526 emission lines were identified. The wavelengths in Table 5 were determined by either fitting gaussians to the top third of the flux of the lines when possible, or by determining the line emission peak by eye. For those emission lines in the Lyα forest, all wavelengths listed were determined by eye. Because the methods used to determine the emission line peaks are fairly inexact, and because the effects of signal to noise and Lyα forest and strong metal absorption hamper the process, we estimate that the peak wavelengths have errors of ±5 Å.

In the process of fitting the quasar continuum level, as noted in Tytler et al. (2004), it was found that emission line features were often required at rest wavelengths of 1071, 1123, and 1176 Å. The values for the rest wavelength, λ_{rest}, listed in Table 5 come either from Table 2 of Telfer et al. (2002) or from Wills et al. (1995), except for the lines near 1071, 1123, and 1176 Å that we discuss below.

In Table 6, we list the redshifts, denoted by z_{eff}, of each quasar as determined by taking the mean of redshifts given by each line observed. We do not use the lines in the first three transitions listed in Table 5, because the errors on these lines are in general larger. To help determine the exact rest wavelengths of the emission lines with wavelengths less than Lyα, Table 6 also provides the rest wavelengths for the first three transitions of Table 5 as determined by dividing their observed wavelengths by $(1 + z_{eff})$. We find the rest wavelengths for these transitions to be 1070.95 ± 1.00, 1123.13 ± 0.51, and 1175.88 ± 0.30 Å. These wavelengths are consistent with the identifications cited in Tytler et al. (2004).

In some cases, we note that the blend of O I and Si II at $\lambda_{rest} = 1306$ Å is dominated by the Si II 1309 transition, and may cause additional errors in the determination of the quasar's redshift. In Table 7, we list those emission lines which were observed in some spectra but are not in Table 5, and where possible, identify the transition responsible for the line. Finally, many quasars in the survey show a shelf like emission feature extending between He II 1640 and O III]. We end with some notes on the emission lines for individual quasars.

Q0743+6601 and Q1122-1648: The C III* emission line is seen in this QSO but is too heavily blended with the wing of Lyα to give a value for the peak position.

Q2134+1531: A broad emission shelf feature is seen, consistent with the feature at $\lambda_{rest} \sim 1065$Å blending with the O VI–Lyβ blend.

Q2140+2403: This is the only QSO for which we do not provide a measurement of the Lyα emission line, due to the effects of the very strong associated absorber near the expected emission line peak.

Q2245+2531: The Si IV–O IV] blend appears to be dominated entirely by Si IV 1393.

4. Acknowledgements

This work was funded in part by grant NAG5-13113 from NASA and by grant AST-0098731 from the NSF. The spectra were obtained from the Lick observatory and we thank the Lick observatory staff. This research has made extensive use of the NASA/IPAC Extragalactic Database (NED) which is operated by JPL, under contract with NASA.

REFERENCES

Barthel, P.D., Tytler, D., and Thomson, B. 1990, A&AS, 82 339

Constantin, A., Shields, J.C., Hamann, F., Foltz, C.B., and Chaffee, F.H. 2002, ApJ, 565, 50

Forster, K., Green, P.J., Aldcroft, T.L., Vestergaard, M., Foltz, C.B., Hewett, P.C. 2001 ApJS, 134, 35

Green, P.J., Aldcroft, T.L., Mathur, S., Wilkes, B.J. and Elvis, M. 2001, ApJ 558, 109

Gregg, M.D., Becker, R.H., White, R.L., Helfand, D.J., McMahon, R.G., and Hook, I.M. 1996, AJ, 112, 407

Hewett, P.C., Foltz, C.B., and Chaffee, F.H. 1995, AJ 109, 1498

Kim, T.S., Viel, M., Haehnelt, M. G., Carswell, R. F., and Cristiani, S. 2004, MNRAS, 347, 355

Kirkman, D., Tytler, D., Suzuki, N., O'Meara, J.M., and Lubin, D. 2003, ApJS, 149, 1

Lanzetta, K.M., Wolfe, A.M., and Turnshek, D.A., 1987, ApJ, 322, 739

Narayanan, D., Hamann, F., Barlow, T. Burbidge, E.M., Cohen, R.D., Junkkarinen, V., and Lyons, R. 2004, ApJ, 601, 715

Laor, A., Bachall, J.N., Jannuzie, B.T., Schneider, D.P., and Green, R.F. 1995, ApJS, 99, 1

Sargent, W.L.W, Steidel, C., and Boksenberg, A. 1988, ApJS, 68, 539

Sargent, W.L.W, Steidel, C., and Boksenberg, A. 1989, ApJS, 69, 703

Scott, J., Bechtold, J., and Dobrzycki, A. 2000, ApJS 130, 37

Suzuki, N., Tytler, D., Kirkman, D., O'Meara, J. M., and Lubin, D., 2003, PASP 115, 1050S

Telfer, R. C., Zheng, W.,Kriss, G. A., and Davidsen, A. F., 2002, ApJ 565,773

Tytler, D., and Fan, X. 1992, ApJS, 79, 1

Tytler, D., Kirkman, D., O'Meara, J.M., Suzuki, N., Orin, A., Lubin, D., Paschos, P., Jena, T., Lin, W., and Norman, M.L. 2004, submitted to ApJ, astro-ph/0403688

Weymann, R.J., Morris, S.L., Foltz, C.B., and Hewett, P.C. 1991, ApJ, 373, 23

Wills, B.J., Netzer, H., and Wills, D. 1985, ApJ, 288, 94

Wills,B. J., Thompson, K. L., Han, M., Netzer,H., Wills,D., Baldwin,J. A., Ferland,G. J., Browne,I. W. A., and Brotherton, M. S. 1995, ApJ, 447, 139

Wisotzki, L., Christlieb, N., Bade, N., Beckmann, V., Koehler, T., Vanelle, C., and Reimers, D. 2000, A&A, 358, 77

This preprint was prepared with the AAS LaTeX macros v5.2.

Table 1. Kast $z \simeq 2$ Spectra of 79 QSOs

Name (1950)	Coordinates (B1950)	Coordinates (J2000)	V	z_{em}[A]	Exposure Time (seconds)
Q0001–2340	00 01 11.50 –23 40 37.0	00 03 44.95 –23 23 54.7	16.70	2.26	1380
Q0014–0420	00 14 09.36 –04 20 57.0	00 16 42.80 –04 04 17.0	16.65	1.96	720
Q0049+0124	00 49 59.56 +01 24 23.3	00 52 33.71 +01 40 40.5	17.00	2.29	2700
Q0109+0213	01 09 42.31 +02 13 53.1	01 12 16.91 +02 29 47.6	17.64	2.34	4800
Q0150–2015	01 50 04.98 –20 15 52.6	01 52 27.30 –20 01 06.0	17.10	2.14	2700
Q0153+7428	01 53 04.33 +74 28 05.6	01 57 34.96 +74 42 43.2	16.00	2.34	1800
Q0218+3707	02 18 02.70 +37 07 04.1	02 21 05.50 +37 20 46.0	17.50	2.41	3600
Q0226–0350	02 26 22.08 –03 50 58.6	02 28 53.21 –03 37 37.1	16.96	2.07	2400
Q0248+3402	02 48 23.35 +34 02 22.0	02 51 27.70 +34 14 41.0	17.70	2.22	4200
Q0348+0610	03 48 36.62 +06 10 15.5	03 51 16.53 +06 19 14.2	17.60	2.05	3600
Q0421+0157	04 21 32.67 +01 57 32.7	04 24 08.56 +02 04 24.9	17.04	2.04	3000
Q0424–1309	04 24 47.81 –13 09 32.9	04 27 07.30 –13 02 53.0	17.50	2.16	4200
Q0450–1310	04 50 54.00 –13 10 39.0	04 53 12.83 –13 05 46.1	16.50	2.25	3600
Q0726+2531	07 26 25.23 +25 31 07.2	07 29 28.47 +25 24 51.9	17.81	2.30	4800
Q0743+6601	07 43 58.60 +66 01 00.0	07 48 46.22 +65 53 31.4	17.00	2.20	3600
Q0748+6105	07 48 01.84 +61 05 35.9	07 52 22.50 +60 57 52.0	17.50	2.49	4200
Q0752+3429	07 52 10.00 +34 29 31.3	07 55 24.00 +34 21 34.0	17.80	2.12	4500
Q0800+3031	08 00 34.43 +30 31 24.1	08 03 42.00 +30 22 55.0	16.70	2.02	3600
Q0836+7104	08 36 21.53 +71 04 22.5	08 41 24.36 +70 53 42.2	16.50	2.18	2400
Q0854+3324	08 54 21.61 +33 24 53.0	08 57 26.95 +33 13 17.2	17.43	2.33	4200
Q0907+3811	09 07 44.95 +38 11 31.9	09 10 54.20 +37 59 15.0	17.30	2.15	3000
Q0936+3653	09 36 32.36 +36 53 35.9	09 39 35.10 +36 40 00.0	17.00	2.02	2400
Q0937–1818	09 37 30.22 –18 18 37.3	09 39 51.10 –18 32 15.0	16.20	2.36	3000
Q1023+3009	10 23 58.86 +30 09 29.9	10 26 48.10 +29 54 12.0	17.10	2.33	3600
Q1103+6416	11 03 03.98 +64 16 21.9	11 06 10.70 +64 00 09.0	15.80	2.20	1800
Q1116+2106	11 16 44.49 +21 06 11.4	11 19 22.90 +20 49 46.0	17.30	2.46	3600
Q1122–1648	11 22 12.28 –16 48 47.4	11 24 42.80 –17 05 17.0	16.50	2.40	2700
Q1130+3135	11 30 06.36 +31 35 24.3	11 32 45.20 +31 18 50.0	17.00	2.29	2400
Q1147+6556	11 47 53.77 +65 56 08.8	11 50 34.50 +65 39 28.0	16.20	2.21	2360

Table 1—Continued

Name (1950)	Coordinates (B1950)	Coordinates (J2000)	V	z_{em}[A]	Exposure Time (seconds)
Q1222+2251	12 22 56.58 +22 51 49.3	12 25 27.40 +22 35 13.0	15.49	2.05	3000
Q1224–0812	12 24 02.65 –08 12 52.8	12 26 37.50 –08 29 29.0	16.83	2.16	2400
Q1224+2905	12 24 57.90 +29 05 23.0	12 27 27.40 +28 48 47.0	17.00	2.25	3600
Q1225+3145	12 25 56.07 +31 45 12.6	12 28 24.96 +31 28 37.6	15.87	2.18	2100
Q1231+2924	12 31 27.08 +29 24 20.8	12 33 55.51 +29 07 48.9	16.84	2.01	2400
Q1247+2657	12 47 39.09 +26 47 27.1	12 50 05.75 +26 31 07.7	15.80	2.03	1200
Q1251+2636	12 51 56.97 +26 36 21.8	12 54 23.08 +26 20 06.5	16.45	2.03	2100
Q1307+4617	13 07 58.49 +46 17 20.8	13 10 11.60 +46 01 24.0	16.74	2.13	3000
Q1312+7837	13 12 30.24 +78 37 44.6	13 13 21.30 +78 21 53.0	16.40	2.00	2400
Q1326+3923	13 26 10.24 +39 23 47.2	13 28 23.70 +39 08 17.0	16.60	2.32	2100
Q1329+4117	13 29 29.82 +41 17 22.7	13 31 41.10 +41 01 58.0	16.30	1.93	4500
Q1331+1704	13 31 10.00 +17 04 25.8	13 33 35.78 +16 49 04.0	16.71	2.08	2700
Q1416+0906	14 16 23.30 +09 06 14.0	14 18 51.09 +08 52 27.1	17.00	2.01	2400
Q1418+2254	14 18 51.06 +22 54 58.3	14 21 08.72 +22 41 17.4	16.60	2.19	1800
Q1422+4224	14 22 37.86 +42 24 01.6	14 24 36.00 +42 10 30.0	17.10	2.21	4200
Q1425–1338	14 25 02.87 –13 38 19.4	14 27 46.40 –13 51 44.0	17.19	2.03	2400
Q1435+6349	14 35 37.25 +63 49 36.0	14 36 45.80 +63 36 37.8	15.00	2.06	1500
Q1517+2556	15 17 08.11 +23 56 52.0	15 19 19.40 +23 46 02.0	16.40	1.90	4500
Q1542+3104	15 42 48.48 +31 04 42.0	15 44 49.00 +30 55 21.0	17.00	2.28	2400
Q1542+5408[B]	15 42 41.88 +54 08 25.6	15 43 59.40 +53 59 03.0	16.00	2.36	1800
Q1559+0853	15 59 57.80 +08 53 53.0	16 02 22.56 +08 45 36.3	16.70	2.26	2400
Q1611+4719	16 11 10.53 +47 19 32.2	16 12 39.90 +47 11 57.0	17.60	2.38	3600
Q1618+5303	16 18 28.71 +53 03 20.0	16 19 42.30 +52 56 13.0	17.50	2.34	4500
Q1626+6433	16 26 20.41 +64 33 32.3	16 26 45.60 +64 26 55.0	15.80	2.31	1800
Q1632+3209	16 32 17.96 +32 09 45.7	16 34 12.78 +32 03 35.4	16.93	2.34	2100
Q1649+4007	16 49 57.45 +40 07 16.7	16 51 37.56 +40 02 18.7	17.18	2.33	2400
Q1703+5350	17 03 01.49 +53 50 57.2	17 04 06.70 +53 46 53.0	17.40	2.37	3600
Q1705+7101	17 05 00.60 +71 01 34.0	17 04 26.08 +70 57 34.7	17.50	2.01	4200
Q1716+4619	17 16 01.69 +46 19 39.0	17 17 26.80 +46 16 31.0	17.10	2.11	2400

Table 1—Continued

Name (1950)	Coordinates (B1950)	Coordinates (J2000)	V	$z_{\rm em}$[A]	Exposure Time (seconds)
Q1720+2501	17 20 49.93 +25 01 20.6	17 22 52.99 +24 58 34.7	17.10	2.25	4000
Q1754+3818	17 54 58.67 +38 18 10.2	17 56 39.70 +38 17 52.0	17.50	2.16	2700
Q1833+5811	18 33 09.83 +58 11 07.8	18 33 57.00 +58 13 34.0	17.00	2.03	1800
Q1834+6117	18 34 46.51 +61 17 07.3	18 35 19.68 +61 19 40.0	17.60	2.27	2700
Q1848+6705	18 48 26.30 +67 05 07.0	18 48 25.35 +67 08 37.2	17.50	2.03	1500
Q2044–1650	20 44 30.78 –16 50 09.4	20 47 19.67 –16 39 05.8	17.36	1.94	3600
Q2103+1843	21 03 50.50 +18 43 46.0	21 06 08.52 +18 55 49.9	16.80	2.21	2400
Q2134+0028	21 34 05.21 +00 28 25.0	21 36 38.59 +00 41 54.2	16.79	1.94	2400
Q2134+1531	21 34 01.07 +15 31 38.2	21 36 23.80 +15 45 07.0	17.30	2.13	3600
Q2135+1326	21 35 40.84 +13 26 19.9	21 38 05.20 +13 39 53.0	17.10	2.30	2700
Q2140+2403	21 40 31.75 +24 03 33.0	21 42 48.50 +24 17 18.0	16.80	2.16	2400
Q2147–0825	21 47 09.10 –08 25 17.9	21 49 48.17 –08 11 16.2	16.18	2.12	2400
Q2150+0522	21 50 54.30 +05 22 08.6	21 53 24.67 +05 36 18.9	17.77	1.98	6000
Q2157–0036	21 57 20.39 –00 36 15.3	21 59 54.45 –00 21 50.3	16.98	1.96	4200
Q2241–2418	22 41 56.68 –24 18 48.8	22 44 40.30 –24 03 02.0	16.95	1.96	1800
Q2245+2531	22 45 03.78 +25 31 39.3	22 47 27.40 +25 47 30.0	17.60	2.16	6000
Q2310+0018[B]	23 10 50.80 +00 18 24.1	23 13 24.45 +00 34 44.5	17.00	2.08	1800
Q2310+3831	23 10 36.18 +38 31 22.7	23 12 58.79 +38 47 42.6	17.50	2.18	3000
Q2320+0755	23 20 03.91 +07 55 33.6	23 22 36.08 +08 12 01.6	17.50	2.08	4500
Q2329-0204	23 29 02.27 –02 04 40.4	23 31 36.33 –01 48 06.5	17.00	1.89	2400
Q2332+2917	23 32 32.03 +29 17 39.5	23 35 01.50 +29 34 15.0	17.60	2.07	6000

[A] This redshift is approximate, from the Lyα peak

[B] BAL QSO

Table 2. Kast $z \simeq 2$ Spectra of 79 QSOs

Name (1950)	Observation Date (Year-Month-Day)	Slit Width (arcseconds)	SNR (1070 Å)	SNR (1170 Å)
Q0001–2340	2001-07-20	3.0	9.04	14.33
Q0014–0420	2001-07-19	3.0	3.19	8.88
Q0049+0124	2001-09-13	3.0	15.24	24.00
Q0109+0213	2001-12-16	2.0	22.73	34.25
Q0150–2015	2001-09-13	3.0	9.26	19.29
Q0153+7428	2001-09-13	3.0	7.53	13.14
Q0218+3707	2002-01-11	2.0	22.08	29.59
Q0226–0350	2003-01-30	2.0	5.45	14.12
Q0248+3402	2002-01-11	2.0	23.27	36.34
Q0348+0610	2003-01-30	2.0	6.02	16.54
Q0421+0157	2001-12-16	2.0	6.19	16.09
Q0424–1309	2002-01-11	2.0	1.71	2.95
Q0450–1310	2003-01-29	2.0	11.99	19.20
Q0726+2531	2003-01-31	2.0	8.94	14.36
Q0743+6601	2001-12-16	2.0	17.36	25.15
Q0748+6105	2001-12-16	2.0	16.62	20.73
Q0752+3429	2003-01-30	2.0	9.18	15.98
Q0800+3031	2002-04-09	1.5	8.09	21.69
Q0836+7104	2002-03-09	2.0	15.92	23.20
Q0854+3324	2003-01-30	2.0	7.29	11.77
Q0907+3811	2003-01-31	2.0	5.42	9.70
Q0936+3653	2003-01-31	2.0	1.24	5.50
Q0937–1818	2003-01-29	2.0	9.59	15.87
Q1023+3009	2002-04-09	1.5	6.28	9.02
Q1103+6416	2003-01-31	2.0	15.16	24.08
Q1116+2106	2002-04-11	1.5	4.44	5.64
Q1122–1648	2003-01-29	2.0	15.23	25.84
Q1130+3135	2003-01-30	2.0	9.69	15.89
Q1147+6556	2002-04-09	1.5	3.54	6.55
Q1222+2251	2003-01-29	2.0	9.24	22.63

Table 2—Continued

Name (1950)	Observation Date (Year-Month-Day)	Slit Width (arcseconds)	SNR (1070 Å)	SNR (1170 Å)
Q1224–0812	2003-01-31	2.0	6.48	12.82
Q1224+2905	2002-04-11	1.5	4.85	6.54
Q1225+3145	2001-05-19	3.0	27.77	45.87
Q1231+2924	2003-01-30	2.0	10.16	22.86
Q1247+2657	2001-05-19	2.0	21.49	45.37
Q1251+2636	2001-05-19	2.0	5.28	15.57
Q1307+4617	2002-03-09	2.0	13.89	24.74
Q1312+7837	2003-01-29	2.0	8.36	20.90
Q1326+3923	2003-01-31	2.0	11.63	16.66
Q1329+4117	2003-07-28	2.0	– [A]	9.49
Q1331+1704	2002-04-11	1.5	7.53	14.35
Q1416+0906	2003-01-29	2.0	3.37	10.42
Q1418+2254	2001-05-19	2.0	11.98	20.80
Q1422+4224	2002-03-09	2.0	5.22	9.53
Q1425–1338	2003-01-30	2.0	1.50	6.34
Q1435+6349	2001-05-19	2.0	8.14	18.13
Q1517+2556	2003-07-29	2.0	– [A]	8.31
Q1542+3104	2001-05-18	2.0	7.83	9.60
Q1542+5408[B]	2001-05-19	2.0	17.20	21.52
Q1559+0853	2001-07-19	3.0	12.65	21.96
Q1611+4719	2002-04-11	1.5	8.94	16.60
Q1618+5303	2001-07-20	3.0	39.17	54.79
Q1626+6433	2001-07-18	3.0	30.55	45.82
Q1632+3209	2001-05-19	2.0	9.99	16.28
Q1649+4007	2001-07-18	3.0	18.98	27.32
Q1703+5350	2001-07-18	3.0	32.88	43.43
Q1705+7101	2001-07-19	2.0	2.74	8.52
Q1716+4619	2001-05-18	3.0	13.29	19.53
Q1720+2501	2001-07-17	3.0	12.49	18.50
Q1754+3818	2001-05-19	2.0	7.90	26.11

Table 2—Continued

Name (1950)	Observation Date (Year-Month-Day)	Slit Width (arcseconds)	SNR (1070 Å)	SNR (1170 Å)
Q1833+5811	2001-05-18	3.0	3.41	8.42
Q1834+6117	2001-05-19	2.0	9.29	14.67
Q1848+6705	2001-05-18	3.0	3.71	8.38
Q2044–1650	2001-07-18	3.0	– [A]	15.63
Q2103+1843	2001-07-17	3.0	32.90	46.93
Q2134+0028	2001-07-19	3.0	– [A]	22.77
Q2134+1531	2001-07-18	3.0	15.16	25.12
Q2135+1326	2001-07-17	3.0	15.78	24.27
Q2140+2403	2001-07-17	3.0	17.08	31.21
Q2147–0825	2003-07-28	2.0	4.36	9.49
Q2150+0522	2003-07-29	2.0	3.97	7.96
Q2157–0036	2003-07-28	2.0	– [A]	20.79
Q2241–2418	2001-07-17	3.0	2.69	10.95
Q2245+2531	2003-07-28	2.0	13.23	26.09
Q2310+0018[B]	2001-07-11	3.0	11.71	20.45
Q2310+3831	2001-07-18	3.0	10.80	17.77
Q2320+0755	2001-07-20	3.0	6.38	12.66
Q2329-0204	2001-07-19	3.0	6.38	12.66
Q2332+2917	2003-07-29	2.0	8.43	21.88

[A] This rest wavelength was not covered by this spectrum

[B] BAL QSO

Table 3. Standard Stars for Flux Calibration

Name	Coordinates (J2000)	V	Spectral Type
G191B2B	05 05 30.6 + 52 49 54	11.78	DAO
Feige 34	10 39 36.7 + 43 06 10	11.18	DO
Feige 67	12 41 51.8 + 17 31 20	11.81	sdO
BD+33d2642	15 51 59.9 + 32 56 55	10.81	B2IV
BD+28d4211	21 51 11.1 + 28 51 52	10.51	0p
Feige 110	23 19 58.4 – 05 09 56	11.82	DOp

Table 4. Strong Absorption Systems

Name (1950)	$z_{\rm abs}$	Ions	Notes
Q0001–2340	2.184	H I, C II, C IV, Al II, Si II, Si IV	
	0.431	Mg II	
Q0014–0420	0.806	Mg II	
Q0049+0124	1.828	H I, C IV, Al II, Al III, Si IV	
	1.663	C IV	
	1.077	Mg II, Fe II	
Q0109+0213	2.212	C IV	
	1.987	C IV	
	1.841	H I, C IV, Al II	
Q0150–2015	2.134	H I, C IV, N V, Si IV	A
	2.010	C IV	
	0.780	Mg II, Fe II	
Q0153+7428	2.346	H I, C IV, N V	A
	0.745	Mg II	
Q0218+3707	2.337	H I, C II, C IV, O I, Al II, Si II, Si IV	
	2.144	C IV	
Q0248+3402	2.167	H I, C IV	
Q0348+0610	2.034	H I, C IV, Si IV	
	2.026	H I, C IV, Si IV	
	1.969	H I, C IV, Si IV	
Q0421+0157	1.637	H I, C IV	
Q0450–1310	2.231	H I, C IV, N IV	A
	2.107	C IV, Si IV	
	2.067	H I, C II, C IV, O I, Si II, Si IV	B
	0.494	Mg II	
Q0726+2531	2.288	H I, C IV, N V, O VI	A
Q0743+6601	1.695	H I, C IV	
	1.650	H I, C IV	
	0.638	Mg II	
Q0748+6105	2.209	H I, C IV	

Table 4—Continued

Name (1950)	$z_{\rm abs}$	Ions	Notes
Q0752+3429	2.068	C IV	
	2.051	H I	c
	1.501	C IV	
	1.063	Mg II, Fe II	
Q0800+3031	1.862	H I	c
Q0854+3324	2.269	H I, C II, C IV, O I, Al II, Si II, Si IV	
Q0836+7104	0.915	Mg II, Fe II	
Q0907+3811	1.820	H I, C IV	
Q0937–1818	0.941	Mg II, Fe II	
Q1103+6416	1.941	C IV	
	1.892	H I, Si IV	
Q1122–1648	0.682	Mg II, Fe II	
Q1130+3135	2.210	C IV	
	2.112	C IV	
	2.021	H I, C II, C IV, Al II, Si II, Si IV	
Q1222+2251	1.936	H I, C II, C IV, Si IV	
	1.486	C IV	
	0.668	Mg II	
Q1224–0812	1.890	H I, C IV	
	1.602	C IV, Al II, Al III, Si II	
Q1225+3145	2.121	C IV	
	1.795	H I, C IV, Al II, Al III, Si II, Si IV	
	1.626	C IV	
Q1231+2924	1.943	C IV	
	1.167	C IV, Al III, Fe II	
Q1247+2657	1.959	H I, C IV, Si IV	
	1.408	C IV	
	1.223	Fe II	
	0.762	Mg II	
Q1326+3923	2.150	H I, C IV, Si IV	

Table 4—Continued

Name (1950)	$z_{\rm abs}$	Ions	Notes
	2.131	H I, Si II, C IV, Al II, Si II, Si IV, Fe II	
	2.088	H I	C
Q1329+4117	1.940	H I, N V, C IV	A
	1.600	H I, C IV	
	1.471	C IV	
	0.922	Mg II	
Q1331+1704	1.776	H I, C II, C IV, O I, Si II, Si IV	B
	0.745	Mg II, Fe II	
Q1418+2254	2.191	H I, C IV, Si IV	A
	1.874	H I, C IV, Si IV	
Q1422+4224	1.951	H I	
Q1435+6349	1.923	H I, C II, C IV, Al II, Si II, Si IV	
Q1517+2356	1.416	C IV	
Q1542+3104	2.076	H I, C II, C IV, Al II, Al III, Si IV	
	1.725	H I, C IV	
Q1542+5408$^{\rm D}$	2.224	H I, C IV, N V, O VI	E
Q1559+0853	2.281	H I, C IV, N V, Si IV	A
	2.252	H I, C II, C IV, Si II	
	2.122	H I, C IV, Si IV	
	1.842	H I, C II, C IV, Al II, Si II	B
Q1618+5303	2.125	H I, C II, Al, II, Si II	
	2.109	H I, C II, C IV, Al II, Si II, Si IV	
Q1626+6433	2.292	H I, C IV, Si IV	
	2.245	H I, C IV	
	2.110	H I, C II, C IV, Al II, Al III, Si IV	
	2.099	C IV	
	2.055	H I, C IV, Si IV	
	1.927	H I, C IV, Al II, Al III, Si II, Si IV	
Q1632+3209	2.350	H I, C IV, Si IV	A
	2.258	C IV	

Table 4—Continued

Name (1950)	$z_{\rm abs}$	Ions	Notes
	2.092	H I, C II, C IV, Al II, Al III, Si II	B
Q1649+4007	1.891	H I, C IV, Al II, Al III, Si II, Si IV	
	1.799	H I, C IV	
	1.638	C IV, Al III	
	0.499	Mg II, Fe II	
Q1703+5350	2.370	H I, C IV, N V, Si IV	A
	2.338	C IV, N V, Si IV	
	2.300	C IV, Si IV	
	1.017	Mg II, Fe II	
	0.699	Mg II, Fe II	
	0.679	Mg II, Fe II	
Q1705+7101	0.713	Mg II, Fe II	
Q1716+4619	2.132	H I, C IV, N V, Si IV	A
	2.049	H I, C IV	
	1.563	C IV	
	0.980	Mg II	
	0.878	Mg II	
Q1720+2501	0.925	Mg II	
	0.817	Mg II	
Q1754+3818	1.784	H I, C II, C IV, O I, Al II, Al III, Si II, Si IV	B
Q1833+5811	2.038	H I, C IV	A
Q1834+6117	2.210	H I, C IV	
	1.100	Mg II, Fe II	
Q2044–1650	1.920	H I, C IV, Si IV	
Q2103+1843	2.110	H I, C IV, Si IV	
	1.964	H I, C IV, Si IV	
Q2134+0028	0.629	Mg II, Fe II	
Q2134+1531	2.045	C IV	
	1.475	C IV	
	1.181	Fe II	

Table 4—Continued

Name (1950)	z_{abs}	Ions	Notes
Q2140+2402	2.163	H I, C II, C IV, O I, Al II, Si II	[A]
	0.962	Mg II	
Q2150+0522	1.990	H I, C IV, N V	[A]
	1.883	H I, C II, O I, Al II, Si II	
	1.730	H I, C IV	
Q2157–0036	1.963	H I, C IV, N V	[A]
	1.650	C IV	
Q2241–2418	0.754	Mg II, Fe II	
Q2245+2531	1.991	H I, C IV	
	0.422	Mg II	
Q2310+0018[D]	2.048	H I, C IV, Si IV	
	1.999	C IV	
	1.971	C IV, N V, Si IV	[E]
	1.902	H I, C IV	
Q2332+2917	2.066	H I, C IV, N V	[A]
	1.874	H I, C IV	
	1.737	C IV, Si IV	
	1.671	C IV	
	0.968	Mg II, Fe II	

[A] Likely associated with QSO

[B] Damped Lyman Alpha system

[C] The strong H I absorption at this redshift shows no apparent metal absorption, and may instead be a blend

[D] BAL QSO

[E] BAL absorption

Table 5. Observed Quasar Emission Line Peak Wavelengths

Name (1950)	N II He II ∼1072	Fe III 1123	C III* 1176	Lyα 1216	N V 1240	Si II 1263	O I Si II 1306	C II 1335	Si IV O IV] 1400	C IV 1549	He II 1640	O III] 1664	Al III 1860	C III] 1909
Q0001–2340	3538.38	···	···	3967.11	···	···	4260.14	4356.04	4540.78	5053.71	···	···	···	···
Q0014–0420	···	···	···	3592.63	3659.56	···	3865.82	3954.43	4137.73	4576.02	···	5558.63	5503.24	5649.53
Q0049+0124	···	···	···	4008.89	···	···	4305.66	···	4612.29	5103.42	···	···	···	···
Q0109+0213	3553.20	3735.64	···	4069.83	4151.09	···	4365.39	···	4672.75	5188.09	5496.71	···	···	···
Q0150-2015	···	3511.28	···	3820.70	···	···	4102.96	4193.47	4399.05	4864.86	5146.26	5236.25	5838.29	···
Q0153+7428	···	···	···	4059.21	4135.19	···	4355.94	4459.03	4667.56	5166.69	5472.18	5577.23	···	···
Q0218+3707	3647.41	···	···	4154.20	···	4318.01	4461.55	4554.49	4775.75	5289.66	5595.30	5670.37	···	···
Q0226–0350	···	3453.79	···	3721.64	···	···	4017.07	4107.23	4288.43	4740.79	5026.28	5090.13	5693.01	5846.98
Q0248+3402	3425.52	3612.57	···	3919.65	···	4061.37	4212.22	4306.73	4512.03	4992.58	···	···	···	···
Q0348+0610	···	···	···	3715.06	···	···	3999.62	···	4284.32	4725.99	4996.42	···	5676.31	4847.23
Q0421+0157	···	···	···	3702.54	···	···	···	···	4267.17	4725.57	···	···	5661.76	5826.89
Q0424–1309	···	···	···	3845.37	···	···	···	···	···	4898.42	···	···	···	···
Q0450–1310	3473.08	···	···	3952.42	···	···	···	···	4537.24	5031.81	5342.14	···	···	···
Q0726+2531	···	···	3880.68	4011.13	···	···	···	···	4617.62	5107.65	···	···	···	···
Q0743+6601	3423.58	3581.04	···	3892.27	···	···	4176.63	4280.26	4472.10	4921.70	···	···	···	···
Q0748+6105	3718.48	···	···	4239.84	4319.47	4404.59	4547.94	4653.01	4872.52	5390.25	···	···	···	···
Q0752+3429	···	···	···	3791.02	3871.45	···	4073.31	4166.24	4364.53	4835.17	···	···	5806.45	···
Q0800+3031	···	···	3553.25	3676.34	3746.62	···	3946.64	···	4231.40	4686.19	4946.86	5036.85	···	5781.41
Q0836+7104	···	3571.99	···	3865.05	···	···	4154.83	···	4453.38	4927.89	···	···	···	···
Q0854+3324	···	···	···	4055.97	4136.37	4218.57	4361.06	4459.36	4672.29	5174.13	5477.93	5558.73	···	···
Q0907+3811	···	···	···	3837.07	···	···	···	4215.64	4417.31	4892.09	···	···	···	···
Q0936+3653	···	···	···	3670.74	···	···	3946.93	···	4229.70	4680.11	···	···	5620.24	5768.60
Q0937–1818	···	···	···	4091.86	4172.38	···	4488.98	···	4707.92	5211.50	···	···	···	···
Q1023+3009	3584.52	3739.53	···	4058.52	4123.40	4202.68	4348.69	···	4661.56	5150.80	···	···	···	···
Q1103+6416	3422.10	···	···	3895.55	···	···	4195.05	4291.91	4462.29	4936.25	···	···	···	···
Q1116+2106	···	···	···	4207.48	···	···	···	···	4823.21	5349.04	···	···	···	···
Q1122–1648	3619.81	3827.42	3999.26	4129.90	4212.21	···	···	···	4754.99	5259.91	···	···	···	···
Q1130+3135	···	···	3876.87	4009.12	4089.53	···	4307.60	···	4615.85	5107.89	5406.98	···	···	···
Q1147+6556	···	···	···	3908.56	···	···	···	···	···	4976.16	···	···	···	···
Q1222+2251	3278.00	···	···	3703.63	3773.37	···	3988.37$^{\mathrm{A}}$	4072.34	4270.70	4717.24	···	···	5665.21	5815.42
Q1224–0812	···	···	···	3842.52	···	···	···	···	···	4853.82	···	···	···	···
Q1224+2905	···	···	···	3958.05	···	···	···	···	4550.13	5029.28	···	···	···	···
Q1225+3145	···	···	···	3868.93	···	···	···	···	···	4918.67	···	···	···	···

Table 5—Continued

Name (1950)	N II He II ∼1072	Fe III 1123	C III* 1176	Lyα 1216	N V 1240	Si II 1263	O I Si II 1306	C II 1335	Si IV O IV] 1400	C IV 1549	He II 1640	O III] 1664	Al III 1860	C III] 1909
Q1231+2924	⋯	⋯	⋯	3665.14	⋯	3806.59	3938.70	4024.38	4220.80	4668.24	⋯	⋯	⋯	5752.26
Q1247+3145	3269.99	3423.82	⋯	3695.20	3769.19	3837.80	3972.72	4058.11	4251.21	4708.09	⋯	5058.89	5657.24	5807.34
Q1251+2636	⋯	3407.63	⋯	3685.96	⋯	⋯	3960.87	⋯	4240.61	4689.39	4966.96	⋯	5649.70	5807.29
Q1307+4617	3352.25	3515.25	⋯	3804.88	⋯	3851.99	4089.20	4192.29	4369.52	4834.06	⋯	⋯	⋯	⋯
Q1312+7837	3245.92	3372.81	⋯	3648.05	3719.52	3796.36	3916.10	⋯	4200.26	4651.81	4920.32	⋯	5583.90	5734.26
Q1326+3923	3551.49	3712.89	⋯	4033.84	4112.78	⋯	⋯	⋯	4642.02	5128.33	⋯	⋯	⋯	⋯
Q1329+4117	⋯	⋯	⋯	3562.93	3633.73	⋯	3828.06	3911.57	4102.21	4543.41	4810.14	4875.95	⋯	5601.05
Q1331+1704	⋯	⋯	⋯	3745.32	3810.23	3891.61	4036.10[A]	⋯	⋯	4767.11	⋯	⋯	⋯	⋯
Q1416+0906	⋯	3378.23	⋯	3657.23	3721.61	3798.49	⋯	⋯	4208.03	4657.94	⋯	⋯	⋯	5739.54
Q1418+2254	3396.61	⋯	⋯	3870.70	⋯	⋯	4158.90	4252.89	4455.25	4927.64	⋯	5297.17	⋯	⋯
Q1422+4224	⋯	⋯	⋯	3904.79	⋯	⋯	⋯	⋯	4491.29	4970.92	⋯	⋯	⋯	⋯
Q1425–1338	⋯	⋯	⋯	3672.73	3735.46	⋯	⋯	⋯	4221.27	4665.66	⋯	⋯	⋯	5751.41
Q1435+6349	3257.09	3439.33	3598.14	3722.15	⋯	⋯	3995.12	⋯	4285.63	4746.52	⋯	⋯	⋯	5847.43
Q1517+2356	⋯	⋯	⋯	3527.90	3593.26	⋯	3791.43	⋯	4058.99	4492.05	⋯	⋯	⋯	5533.73
Q1542+3104	⋯	⋯	3851.17	3996.24	⋯	⋯	⋯	⋯	4585.67	5072.14	⋯	⋯	⋯	⋯
Q1542+5408[B]	3601.08	⋯	⋯	4093.20	⋯	⋯	4400.36	⋯	4707.39	⋯	⋯	⋯	⋯	⋯
Q1559+0853	⋯	⋯	⋯	3974.32	4052.14	⋯	4267.77	⋯	4572.26	5054.89	⋯	⋯	⋯	⋯
Q1611+4719	⋯	⋯	⋯	4122.07	⋯	⋯	4406.98	⋯	4693.79	5189.04	⋯	⋯	⋯	⋯
Q1618+5303	3569.20	3760.92	⋯	4072.03	⋯	⋯	4374.11	⋯	4686.69	5182.64	⋯	5579.00	⋯	⋯
Q1626+6433	3531.17	3715.87	⋯	4022.81	4091.56	4176.64	4324.98[A]	4419.10	4637.36	5123.94	⋯	⋯	⋯	⋯
Q1632+3209	3578.04	⋯	⋯	4067.78	4149.19	⋯	4370.22	⋯	4678.08	5173.28	⋯	⋯	⋯	⋯
Q1649+4007	⋯	⋯	3919.90	4057.01	4136.65	⋯	4357.44	⋯	4676.83	5171.99	5470.39	5553.93	⋯	⋯
Q1703+5350	⋯	⋯	⋯	4093.11	4173.13	4250.98	4395.64	4502.46	4716.50	5214.11	5512.69	5604.67	⋯	⋯
Q1705+7101	⋯	⋯	⋯	3659.56	3730.10	⋯	⋯	⋯	4211.27	4661.54	⋯	⋯	⋯	5745.21
Q1716+4519	⋯	3488.73	⋯	3778.86	⋯	⋯	4066.54[A]	4150.57	4348.35	4791.79	⋯	⋯	⋯	⋯
Q1720+2501	3478.00	⋯	⋯	3951.56	4025.86	⋯	⋯	⋯	4543.90	5033.93	5332.45	⋯	⋯	⋯
Q1754+3818	⋯	3547.88	⋯	3834.49	⋯	⋯	4116.77	4210.43	4412.27	4884.23	⋯	⋯	⋯	⋯
Q1833+5813	3251.34	⋯	⋯	3684.65	⋯	⋯	3965.69	⋯	4232.23	4681.22	⋯	⋯	⋯	5771.15
Q1834+6117	3521.56	3672.31	3850.92	3981.05	4060.70	4136.95	4273.09	⋯	4563.05	5075.61	5373.39	⋯	⋯	⋯
Q1848+6705	⋯	3390.94	3555.86	3682.76	3746.20	⋯	3947.47	4036.26	4228.47	4678.83	⋯	⋯	⋯	5779.84
Q2044–1650	⋯	3295.56	⋯	3572.47	3644.85	⋯	⋯	⋯	4109.97	4552.26	4820.87	⋯	⋯	5607.79
Q2103+1843	⋯	⋯	⋯	3898.96	3978.71	⋯	4187.53	4281.44	4488.13	4970.02	5259.21	5338.05	⋯	⋯
Q2134+0028	⋯	⋯	⋯	3574.56	⋯	⋯	3843.43	3921.12	4114.54	4548.77	4821.31	⋯	⋯	5610.11

Table 5—Continued

Name (1950)	N II He II ~1072	Fe III 1123	C III* 1176	Lyα 1216	N V 1240	Si II 1263	O I Si II 1306	C II 1335	Si IV O IV] 1400	C IV 1549	He II 1640	O III] 1664	Al III 1860	C III] 1909
Q2134+1531	···	3525.60	3681.23	3807.99	3882.19	3954.58	4090.31	4180.85	4383.55	4854.16	5137.08	5217.82	···	···
Q2135+1326	3525.60	3705.06	···	4007.78	4073.03	4160.02	4308.69	4408.41	4607.32	5092.70	···	···	···	···
Q2140+2403	···	···	···	···	···	···	4132.89	···	4426.43	4893.11	···	···	···	···
Q2147–0825	···	···	···	3796.25	···	···	4079.66	···	4366.70	4836.31	···	···	···	···
Q2150+0522	···	···	···	3621.48	3694.10	···	···	···	4169.89	4628.60	4887.75	···	5539.35	5674.18
Q2157-0036	···	···	···	3601.79	3670.88	···	3866.89	···	4144.75	4586.64	···	4929.17	5505.82	5654.17
Q2241–2418	···	3322.16	···	3597.83	3666.74	···	3866.26	···	4143.69	4583.13	···	4926.35	···	5647.36
Q2245+2531	···	3547.02	···	3837.61	3912.05	···	···	···	···	4892.12	5175.12	5250.30	···	···
Q2310+0018[B]	3301.11	···	···	3745.31	3812.39	3892.14	4026.28	···	4319.99	4769.51	5052.07	···	5728.50	···
Q2310+3831	3412.83	3568.49	···	3861.60	3935.84	···	4151.16[A]	···	4449.94	4923.74	···	5286.97	5728.51	···
Q2320+0755	3309.54	···	···	3753.69	3824.23	···	4035.43	···	4322.25	4776.34	5057.92	···	···	···
Q2329–0204	···	···	3406.31	3520.29	3589.02	···	3780.76	···	4052.15	4482.69	4742.46	4812.01	···	5523.808
Q2332+2917	3267.11	···	···	3732.02	···	···	4017.15	···	4294.97	4739.35	···	···	···	5841.71

[A] The O I–Si II blend in this line is dominated by the Si II 1309 transition

[B] BAL QSO

Table 6. Effective Redshifts & Calculated Rest Wavelengths

Name (1950)	z_{eff}	λ_{rest} (1071Å)	λ_{rest} (1123Å)	λ_{rest} (1176Å)
Q0001–2340	2.2587	1085.84	⋯	⋯
Q0014–0420	1.9996	⋯	⋯	⋯
Q0049+0124	2.2957	⋯	⋯	⋯
Q0109+0213	2.3460	1061.94	1116.46	⋯
Q0150–2015	2.1414	⋯	1117.74	⋯
Q0153+7428	2.3383	⋯	⋯	⋯
Q0218+3707	2.4136	1068.50	⋯	⋯
Q0226–0350	2.0649	⋯	1126.89	⋯
Q0248+3402	2.2227	1062.93	1120.97	⋯
Q0348+0610	1.9809	⋯	⋯	⋯
Q0421+0157	2.0480	⋯	⋯	⋯
Q0424–1309	2.1623	⋯	⋯	⋯
Q0450–1310	2.2493	1068.88	⋯	⋯
Q0726+2531	2.2981	⋯	⋯	1176.64
Q0743+6601	2.1954	1071.42	1120.70	⋯
Q0748+6105	2.4836	1067.41	⋯	⋯
Q0752+3429	2.1200	⋯	⋯	⋯
Q0800+3031	2.0233	⋯	⋯	1175.30
Q0836+7104	2.1805	⋯	1123.08	⋯
Q0854+3324	2.3388	⋯	⋯	⋯
Q0907+3811	2.1567	⋯	⋯	⋯
Q0936+3653	2.0211	⋯	⋯	⋯
Q0937–1818	2.3789	⋯	⋯	⋯
Q1023+3009	2.3292	1076.69	1123.25	⋯
Q1103+6416	2.2009	1069.09	⋯	⋯
Q1116+2106	2.4528	⋯	⋯	⋯
Q1122–1648	2.3963	1065.80	1126.93	1177.52
Q1130+3135	2.2975	⋯	⋯	1175.71
Q1147+6556	2.2134	⋯	⋯	⋯
Q1222+2251	2.0476	1075.59	⋯	⋯

Table 6—Continued

Name (1950)	z_{eff}	λ_{rest} (1071Å)	λ_{rest} (1123Å)	λ_{rest} (1176Å)
Q1224–0812	2.1467	···	···	···
Q1224+2905	2.2506	···	···	···
Q1225+3145	2.1785	···	···	···
Q1231+2924	2.0143	···	···	···
Q1247+3145	2.0399	1075.70	1126.31	···
Q1251+2636	2.0327	···	1123.65	···
Q1307+4617	2.1154	1076.04	1128.36	···
Q1312+7837	2.0015	1081.44	1123.71	···
Q1326+3923	2.3151	1071.30	1119.98	···
Q1329+4117	1.9314	···	···	···
Q1331+1704	2.0804	···	···	···
Q1416+0906	2.0060	···	1123.84	···
Q1418+2254	2.1834	1066.99	···	···
Q1422+4224	2.2095	···	···	···
Q1425–1338	2.0146	···	···	···
Q1435+6349	2.0617	1063.82	1123.34	1175.21
Q1517+2356	1.9000	···	···	···
Q1542+3104	2.2788	···	···	1174.58
Q1542+5408^{A}	2.3660	1069.85	···	···
Q1559+0853	2.2667	···	···	···
Q1611+4719	2.3667	···	···	···
Q1618+5303	2.3488	1065.81	1123.05	···
Q1626+6433	2.3081	1067.42	1123.25	···
Q1632+3209	2.3438	1070.06	···	···
Q1649+4007	2.3374	···	···	1174.54
Q1703+5350	2.3667	···	···	···
Q1705+7101	2.0089	···	···	···
Q1716+4519	2.1060	···	1123.24	···
Q1720+2501	2.2486	1070.60	···	···
Q1754+3818	2.1528	···	1125.30	···

Table 6—Continued

Name (1950)	z_{eff}	λ_{rest} (1071Å)	λ_{rest} (1123Å)	λ_{rest} (1176Å)
Q1833+5813	2.0270	1074.12	···	···
Q1834+6117	2.2726	1076.06	1122.12	1176.70
Q1848+6705	2.0235	···	1121.54	1176.09
Q2044–1650	1.9382	···	1121.64	···
Q2103+1843	2.2072	···	···	···
Q2134+0028	1.9391	···	···	···
Q2134+1531	2.1322	···	1125.59	1175.28
Q2135+1326	2.2935	1070.48	1124.97	···
Q2140+2403	2.1617	···	···	···
Q2147–0825	2.1217	···	···	···
Q2150+0522	1.9792	···	···	···
Q2157–0036	1.9611	···	···	···
Q2241–2418	1.9591	···	1122.70	···
Q2245+2531	2.1560	···	1123.91	···
Q2310+0018^{A}	2.0805	1071.60	···	···
Q2310+3831	2.1771	1074.19	1123.18	···
Q2320+0755	2.0860	1072.45	···	···
Q2329–0204	1.8937	···	···	1177.14
Q2332+2917	2.0665	1065.42	···	···
N	79	29	27	11
Mean λ_{rest}	2.1661	1070.95	1123.17	1175.88
σ		5.41	2.65	1.01
$\sigma/\sqrt{N}$		1.00	0.51	0.30

^{A}BAL QSO

Table 7. Additional Emission Lines

Name (1950)	λ_{obs} (Å)	λ_{rest}[A] (Å)	Transition
Q1023+3009	3978	1195	Si II
Q1222+2251	4478	1469	···
Q1225+3145	4196	1320	···
Q1307+4617	4593	1474	···
Q1312+7837	5253	1750	N III]
Q1425–1338	3431	1138	···
Q1517+2556	4663	1608	Fe II
Q1559+0853	3691	1130	···
Q1611+4719	4407	1309	Si II
Q1705+7101	3364	1118	···
Q1716+4519	5361	1726	···
Q2044–1650	3367	1146	···
Q2134+0028	3480	1184	···
Q2134+1531	5607	1790	···
Q2140+2403	3570	1129	···
Q2245+2531	3667	1162	···
Q2310+0018[B]	5514	1790	···

[A] Obtained using z_{eff} from Table 6

[B] BAL QSO

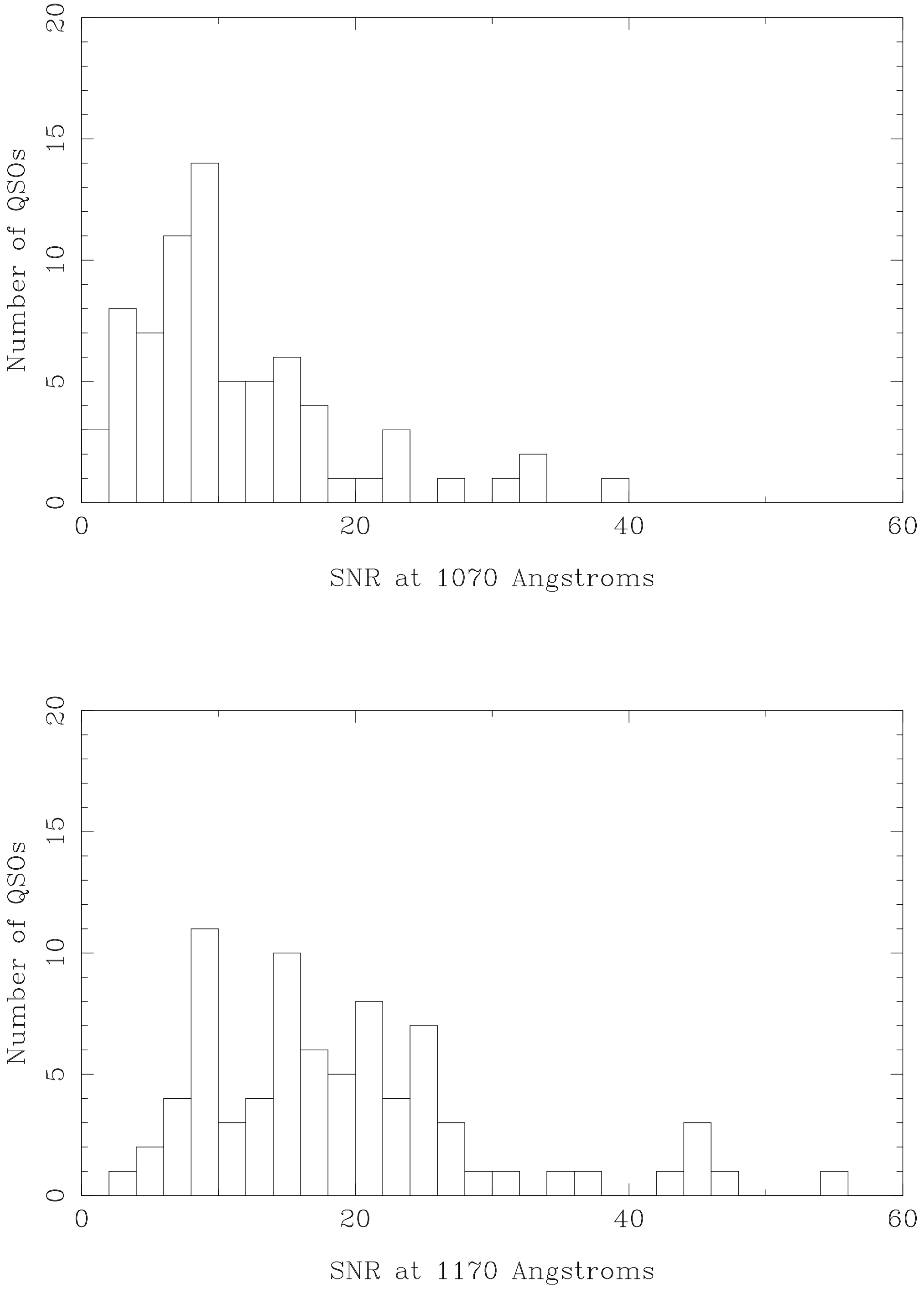

Fig. 1.— Signal to noise distribution for the 79 quasars in the survey. The upper panel shows the signal to noise distribution for the data sampled over 20 Å centered at 1070 Å, while the lower panel shows the distribution sampled over 20 Å centered at 1170 Å.

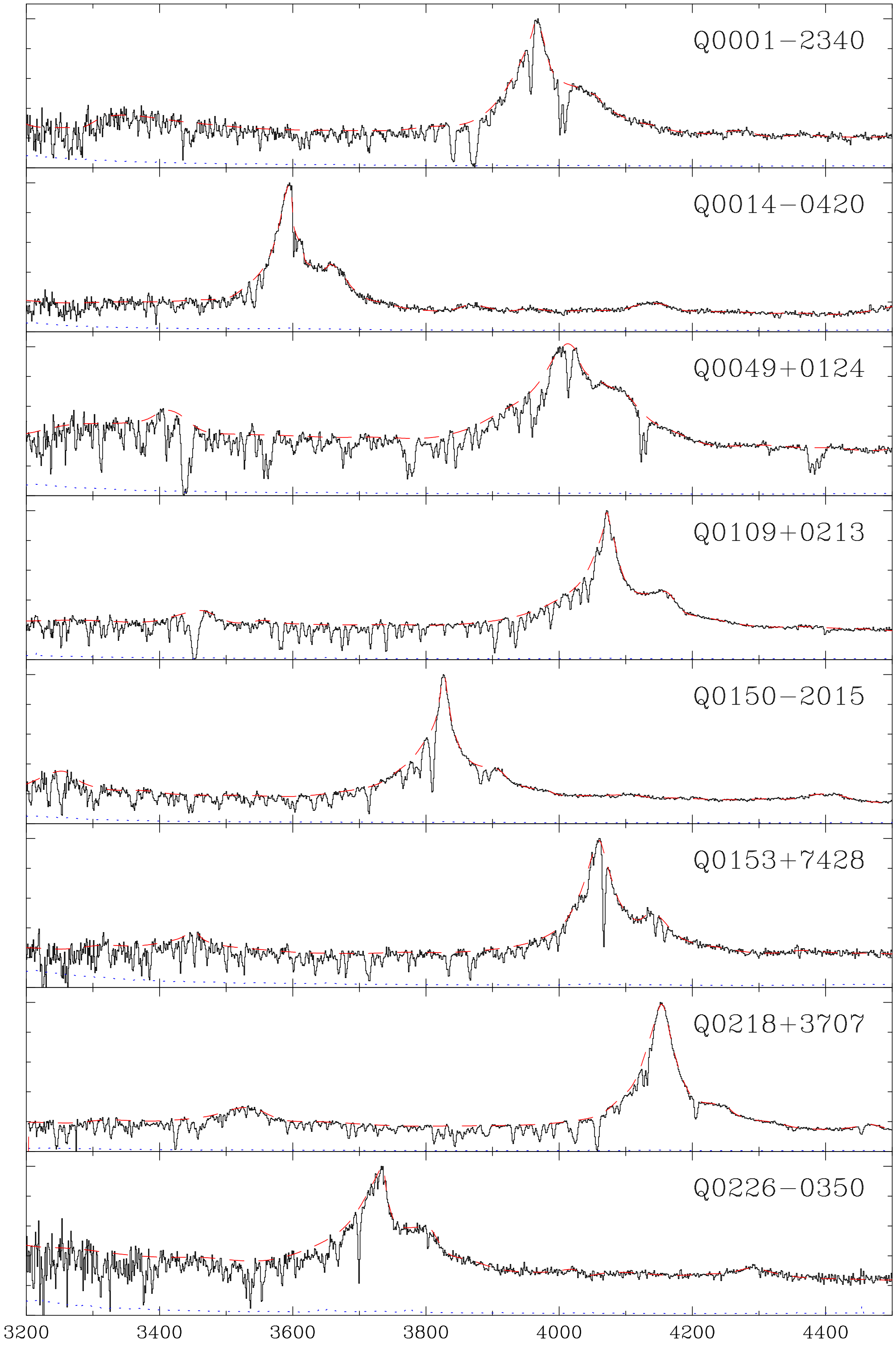

Fig. 2.— Blue camera exposures of the QSOs in the Kast $z \simeq 2$ survey. For each QSO, the flux is shown as the thick line, the 1σ error in the flux as the dotted line, and the dashed line represents the fit to the continuum level. The **y** axis is the flux level, in erg sec^{-1} cm^{-2} $\mathrm{Å}^{-1}$, on a linear scale with zero flux at the bottom, and the **x** axis is in units of Å.

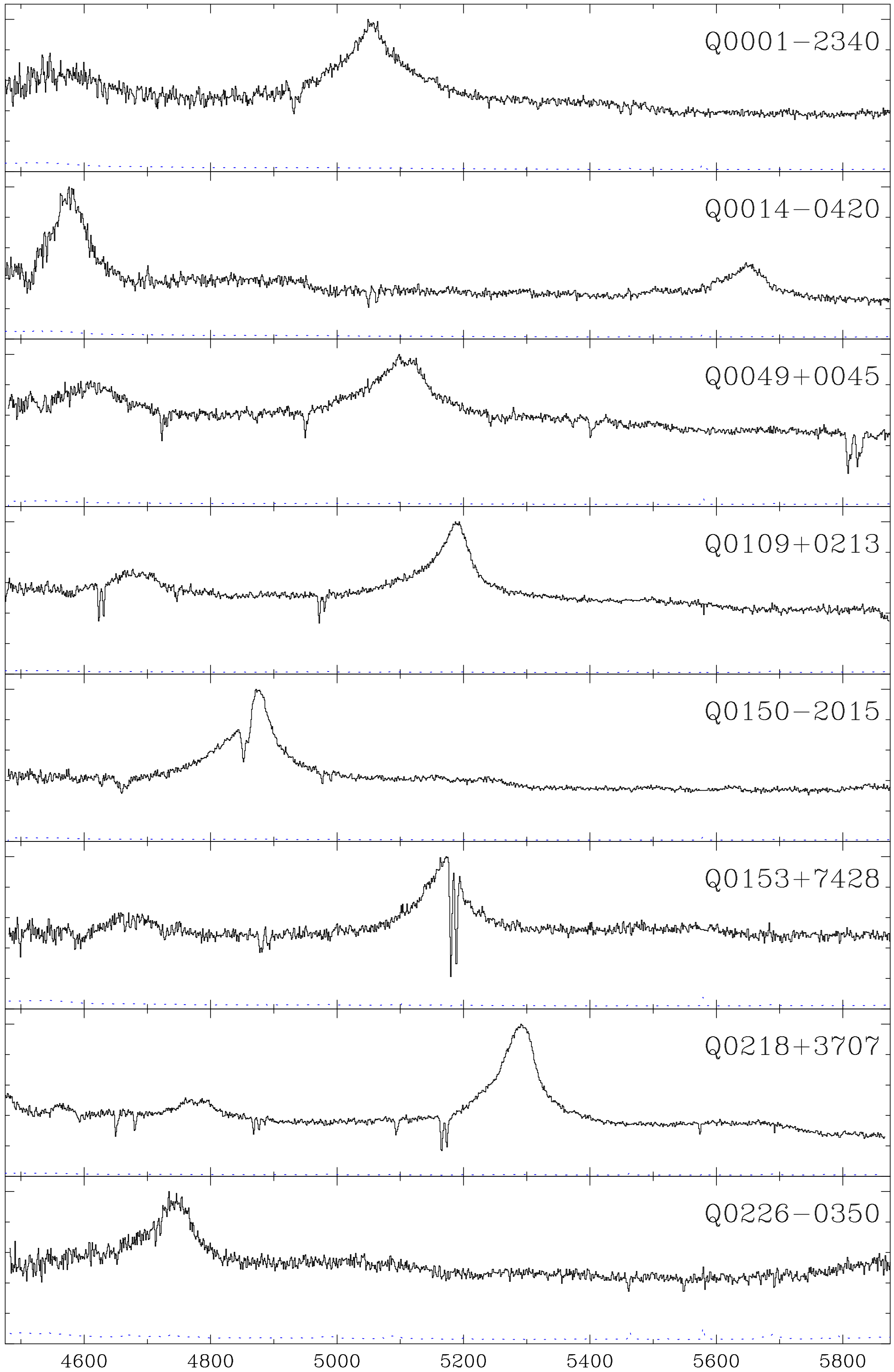

Fig. 3.— Same as for Figure 2, but for the red camera.

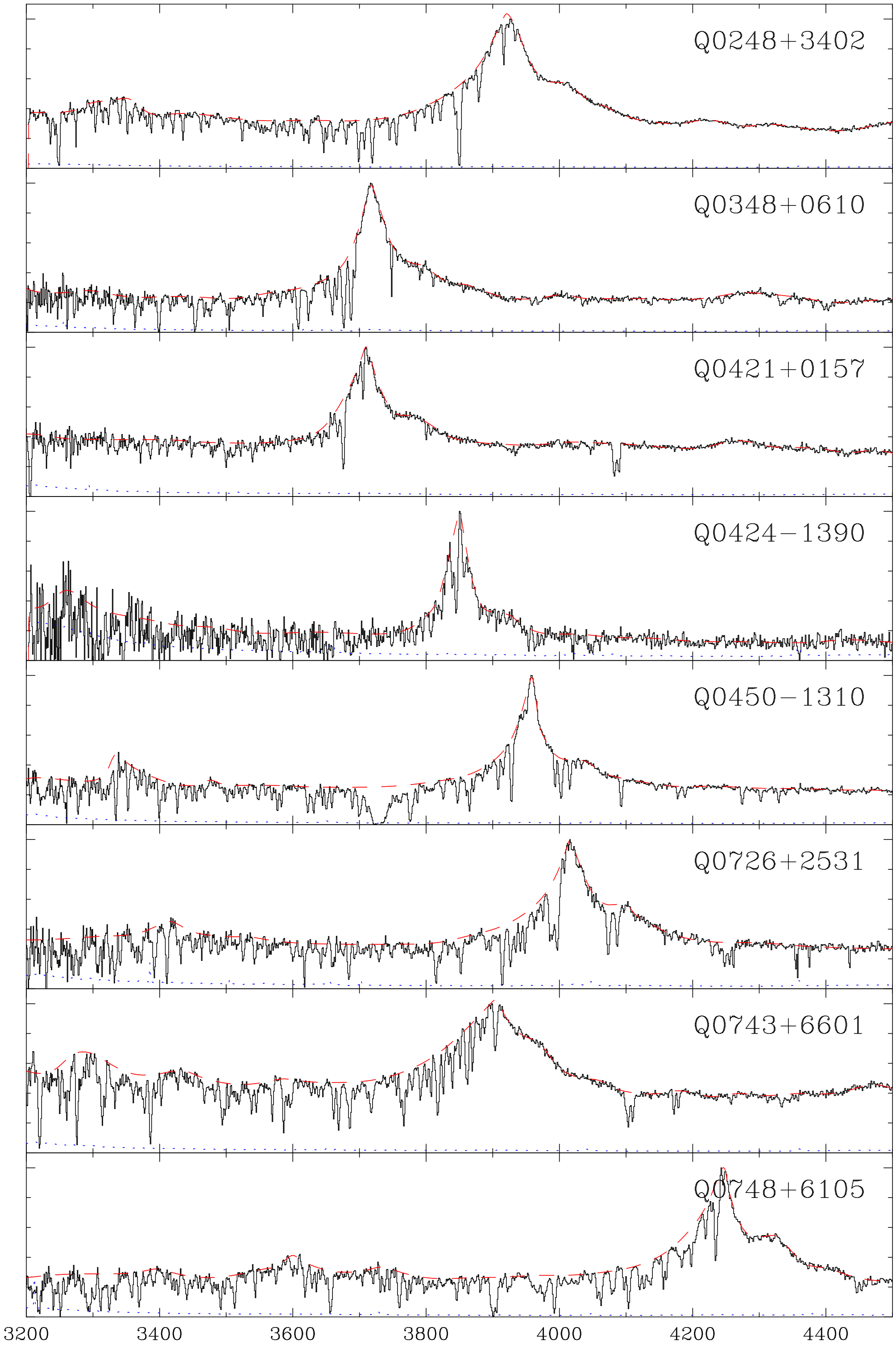

Fig. 4.— Same as for Figure 2.

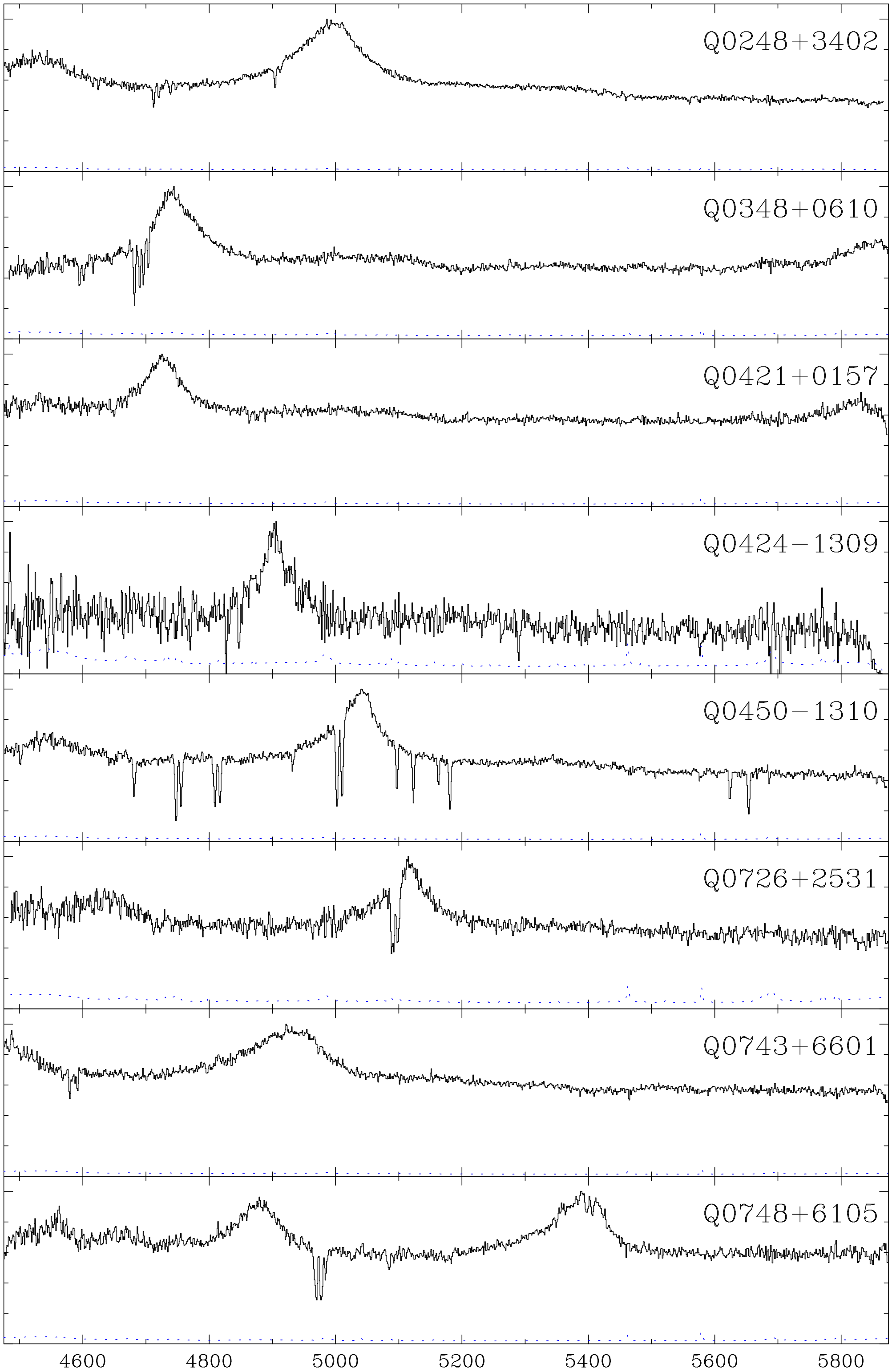

Fig. 5.— Same as for Figure 3.

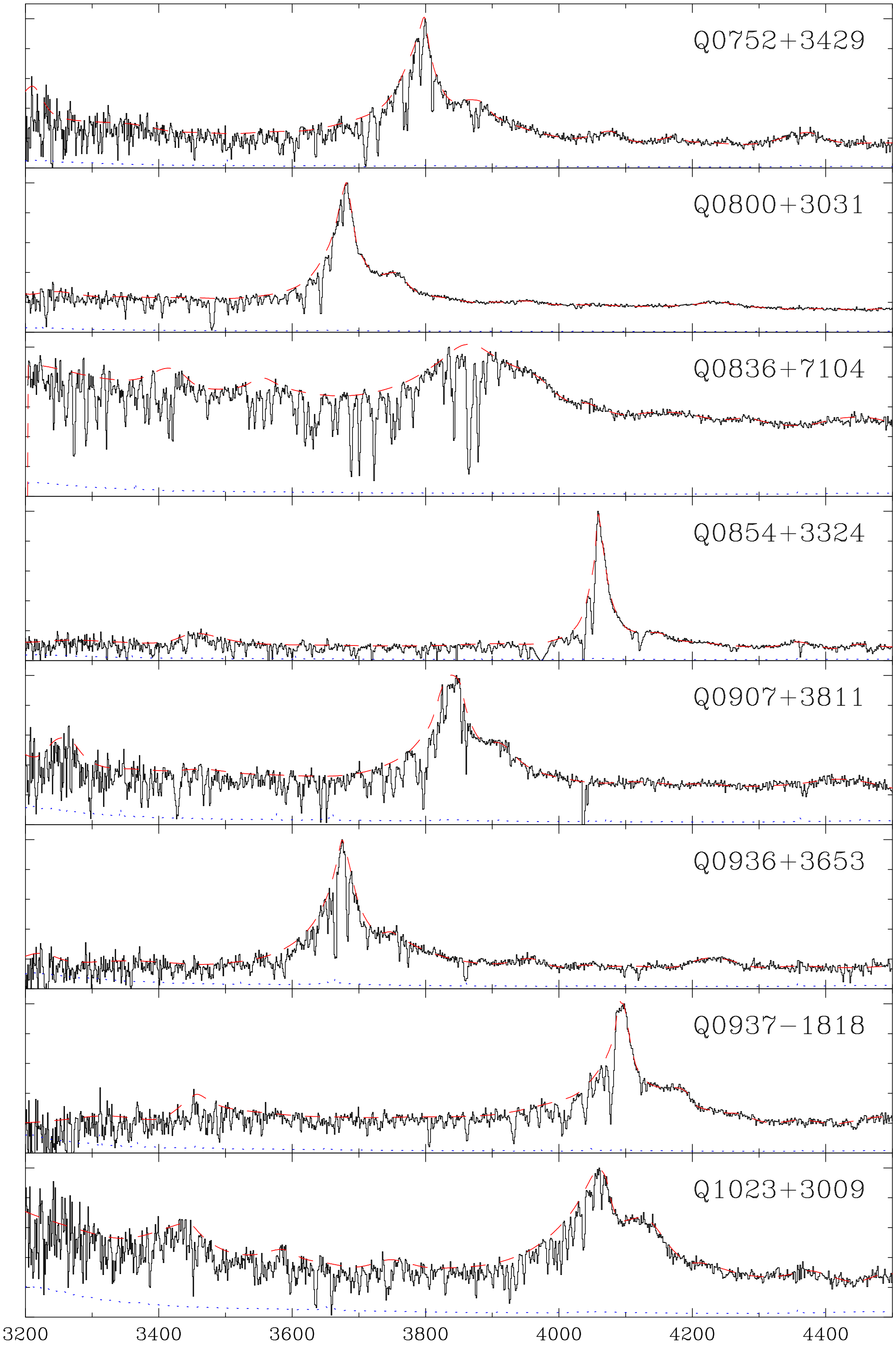

Fig. 6.— Same as for Figure 2.

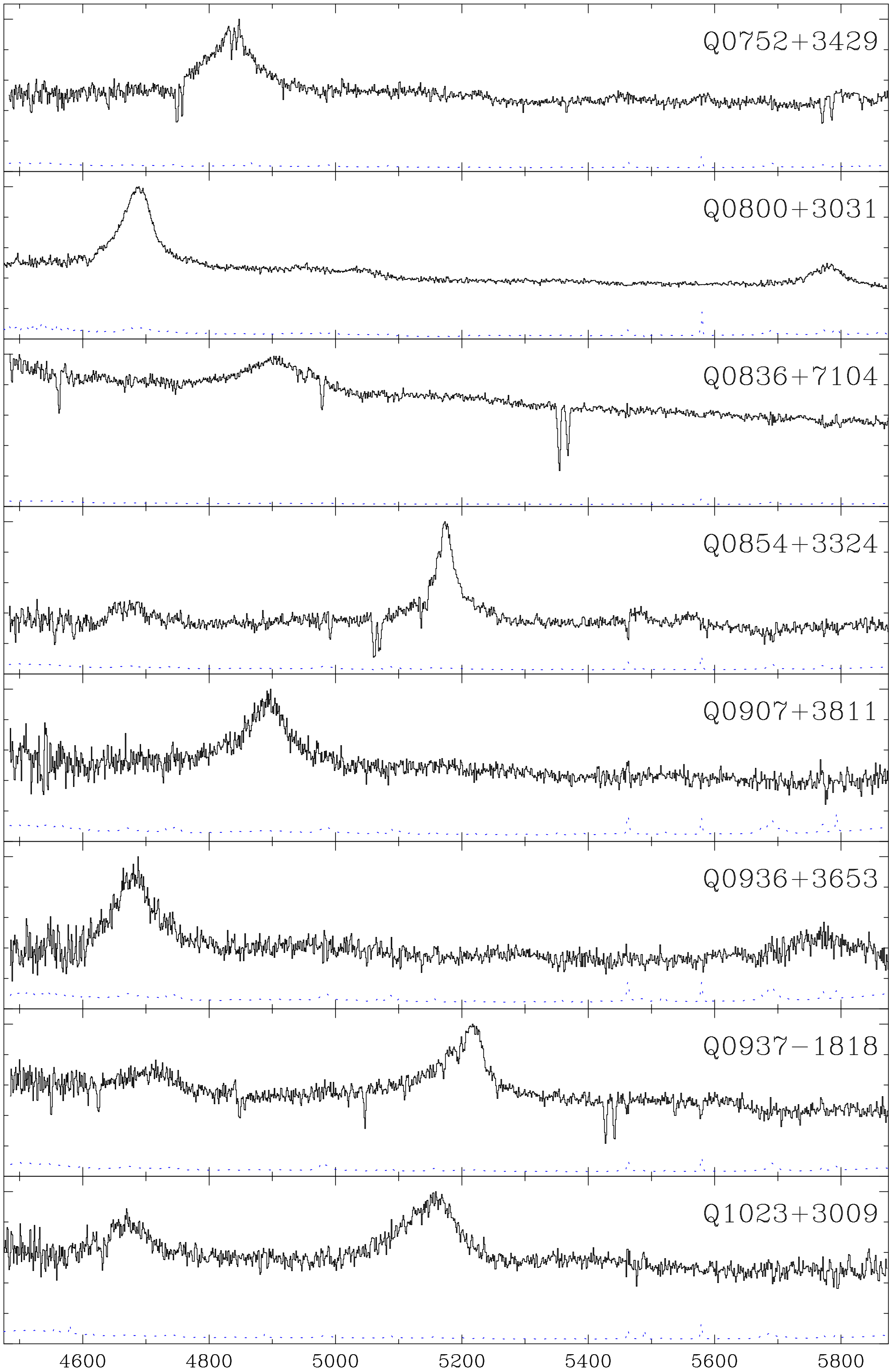

Fig. 7.— Same as for Figure 3.

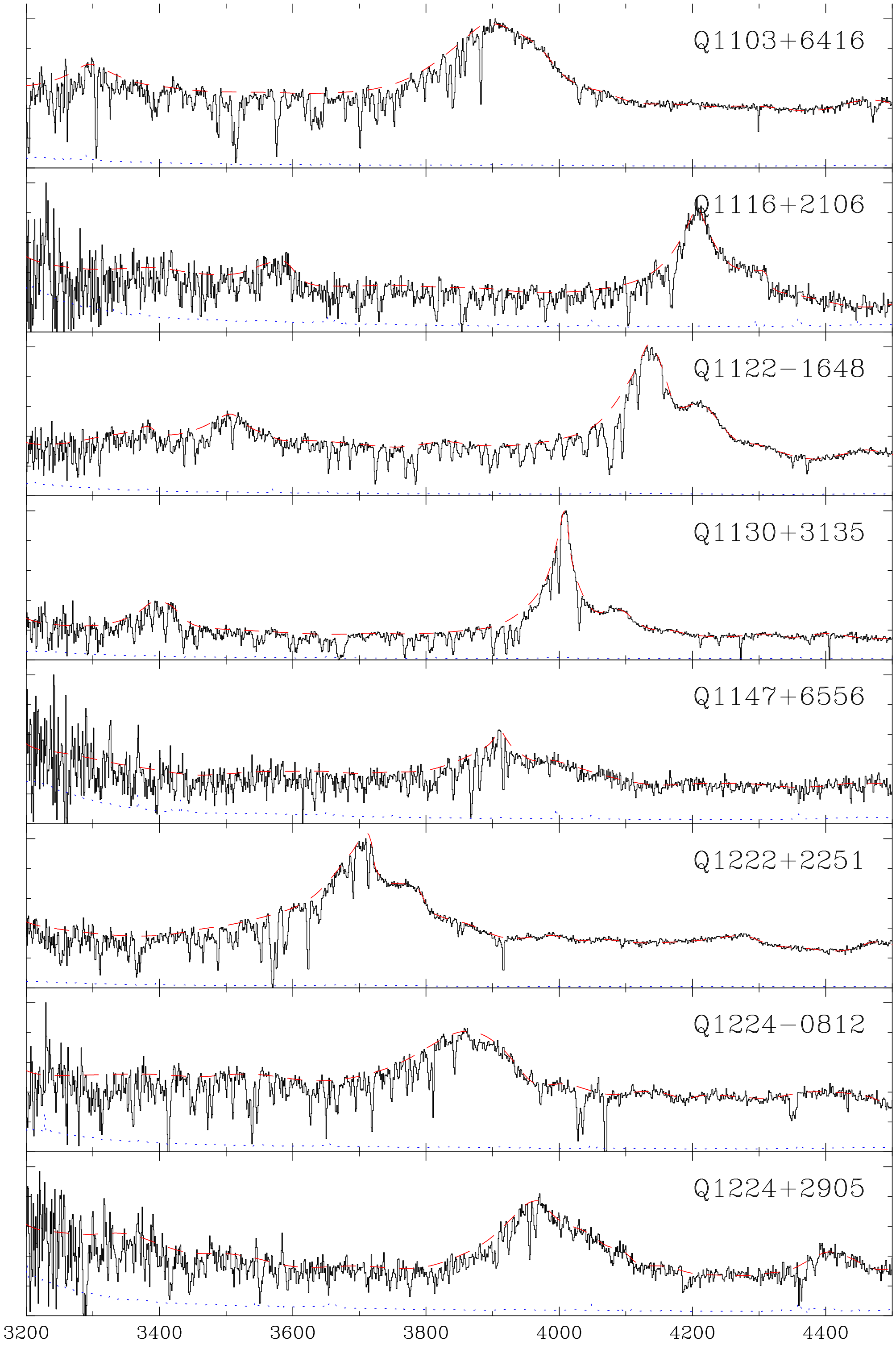

Fig. 8.— Same as for Figure 2.

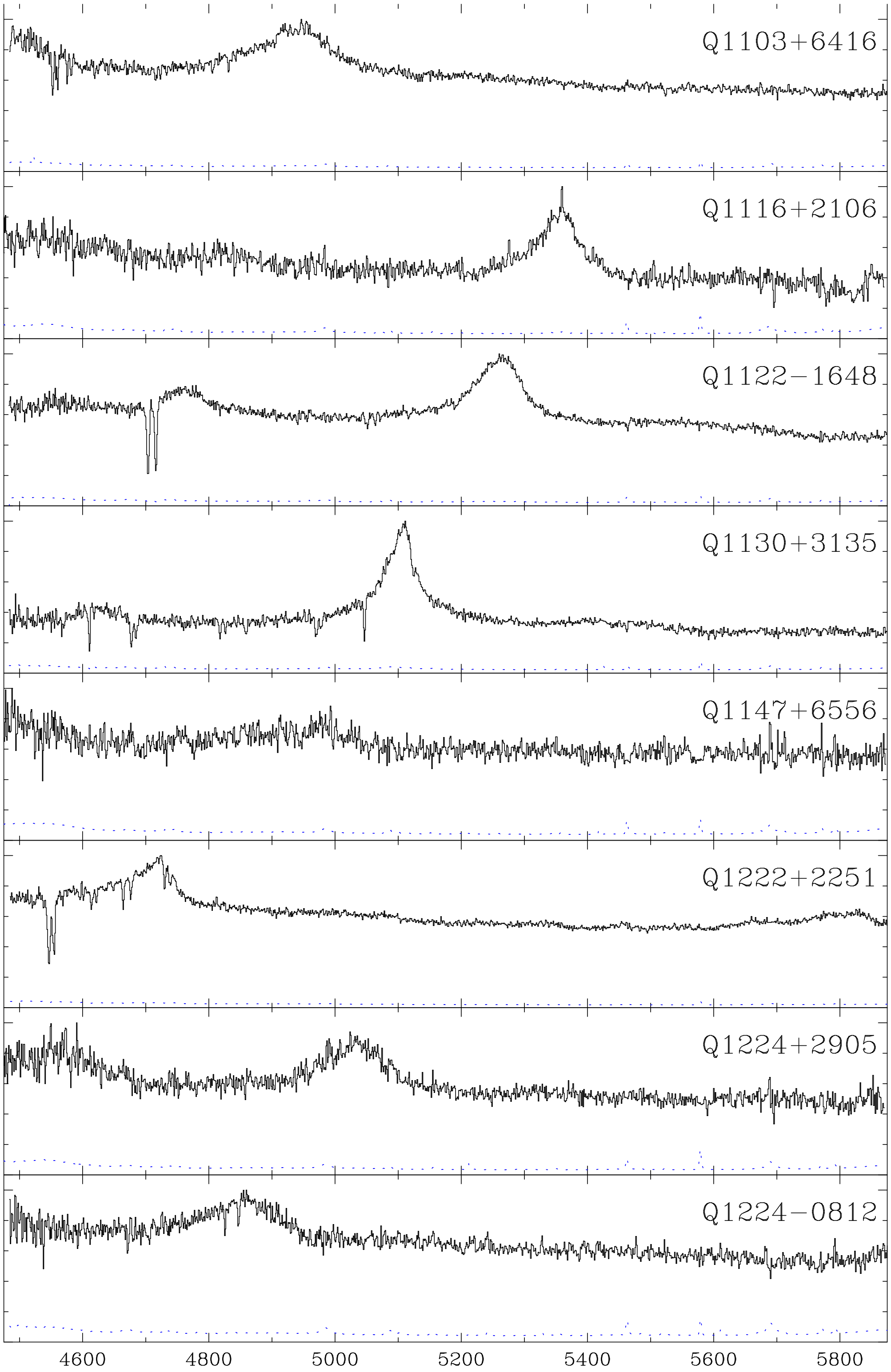

Fig. 9.— Same as for Figure 3.

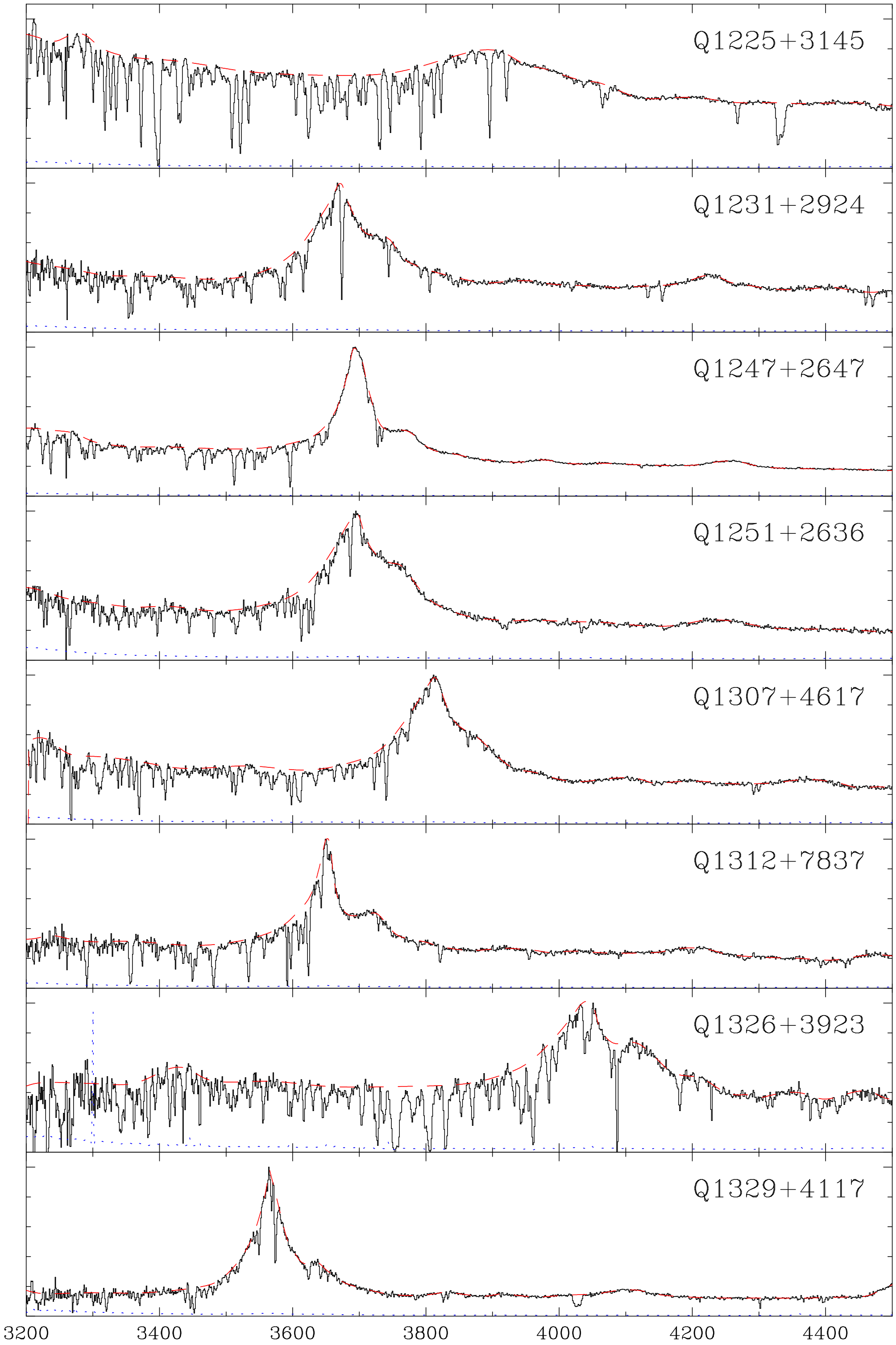

Fig. 10.— Same as for Figure 2.

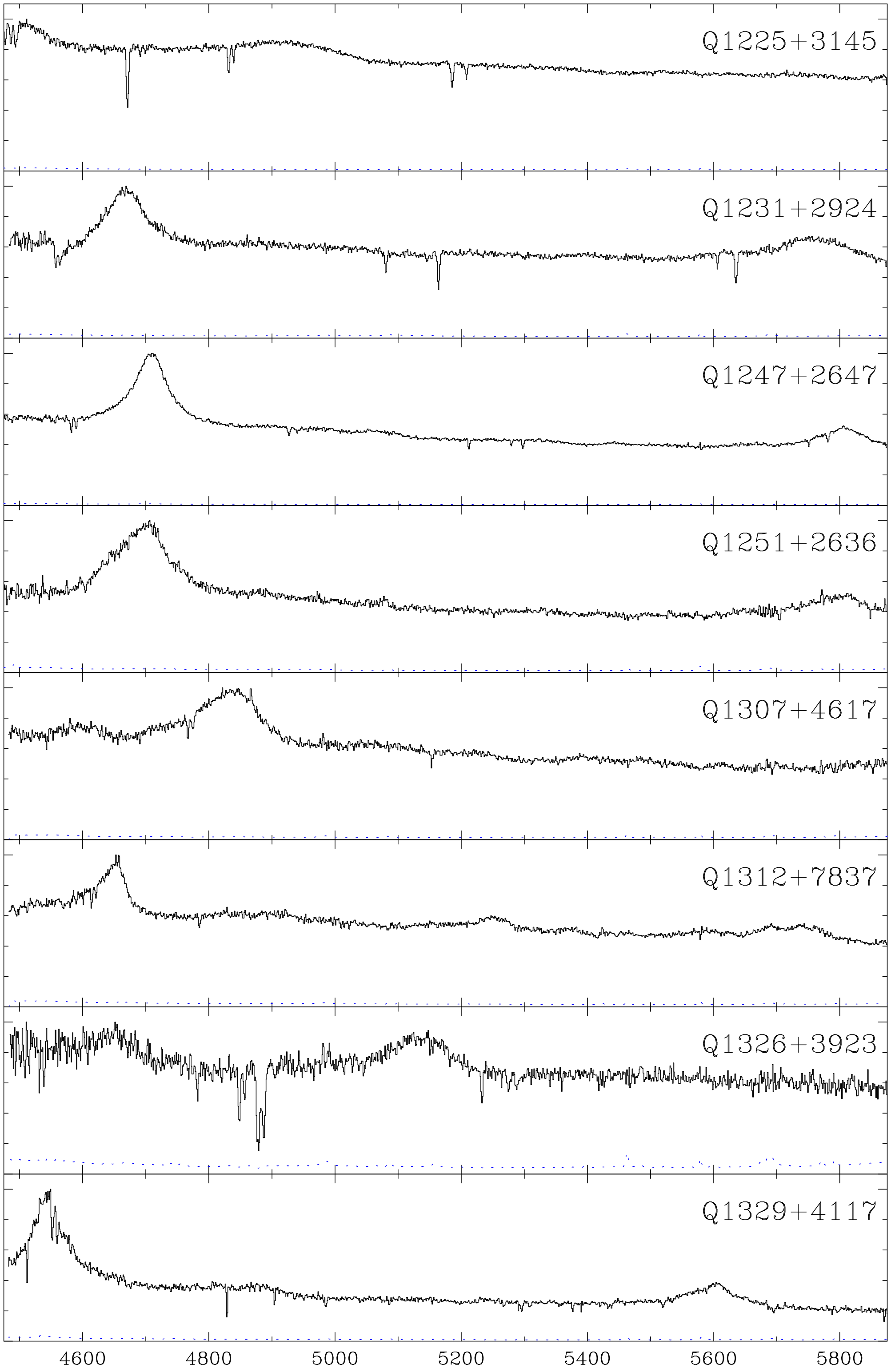

Fig. 11.— Same as for Figure 3.

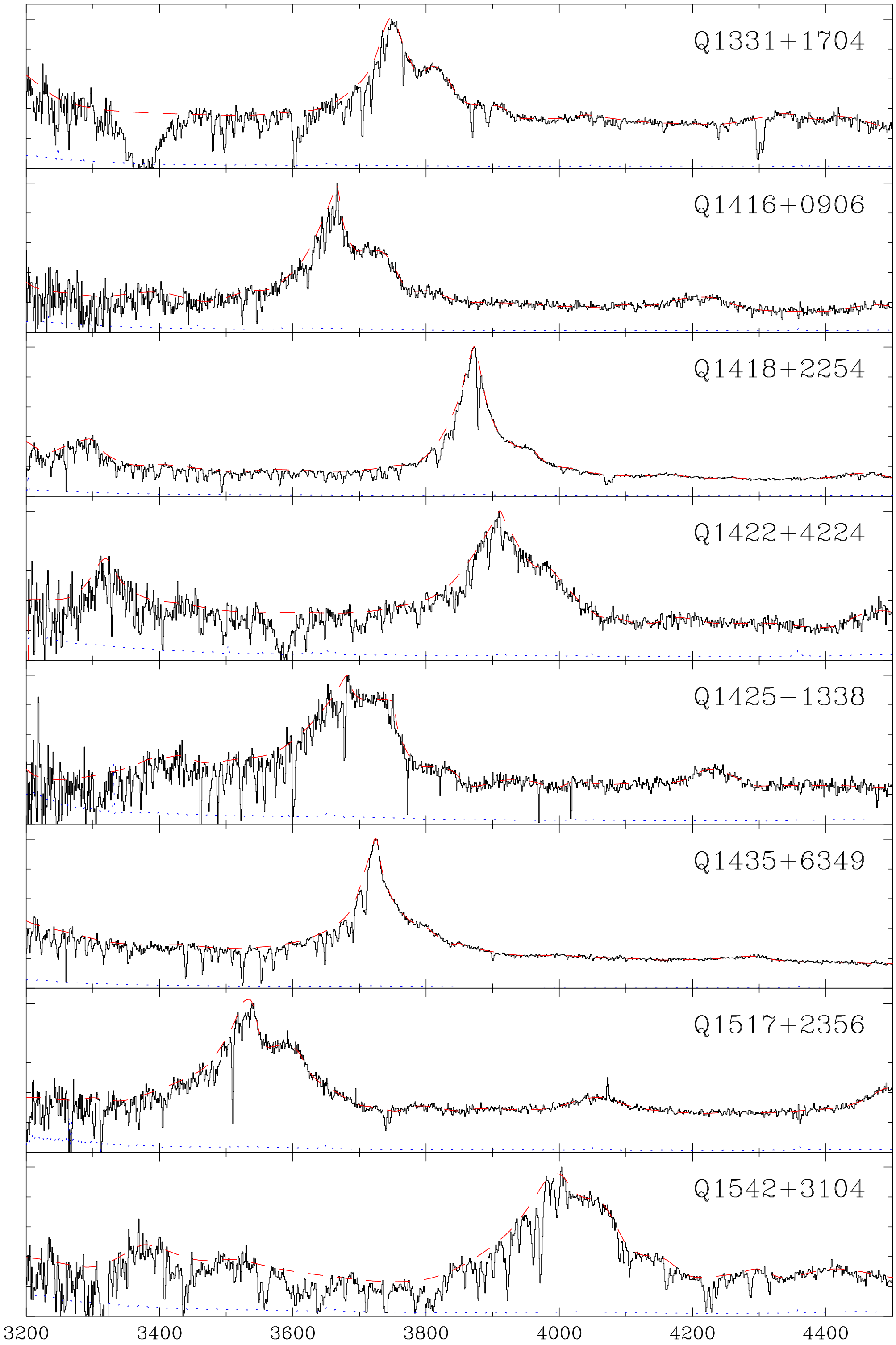

Fig. 12.— Same as for Figure 2.

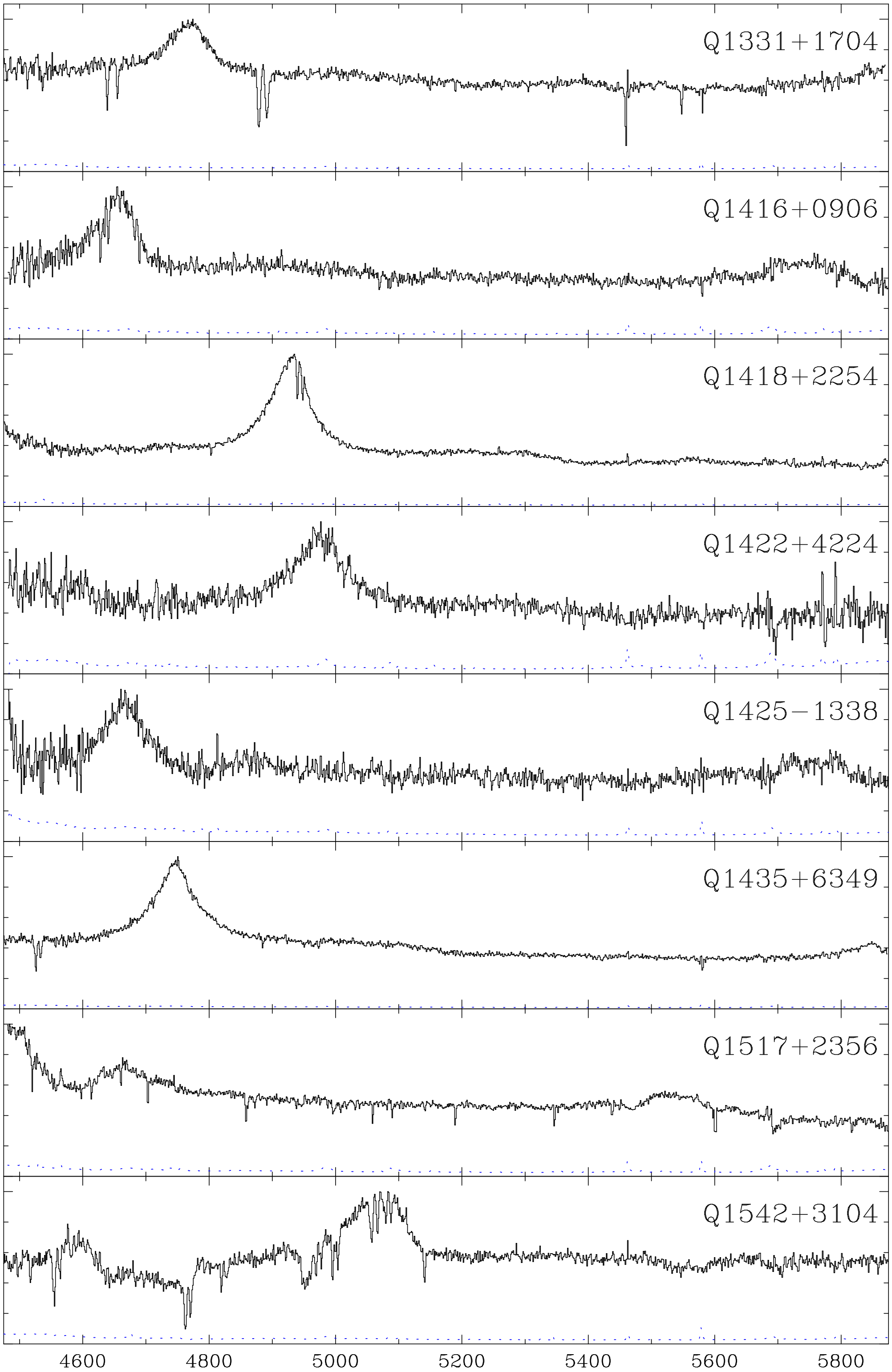

Fig. 13.— Same as for Figure 3.

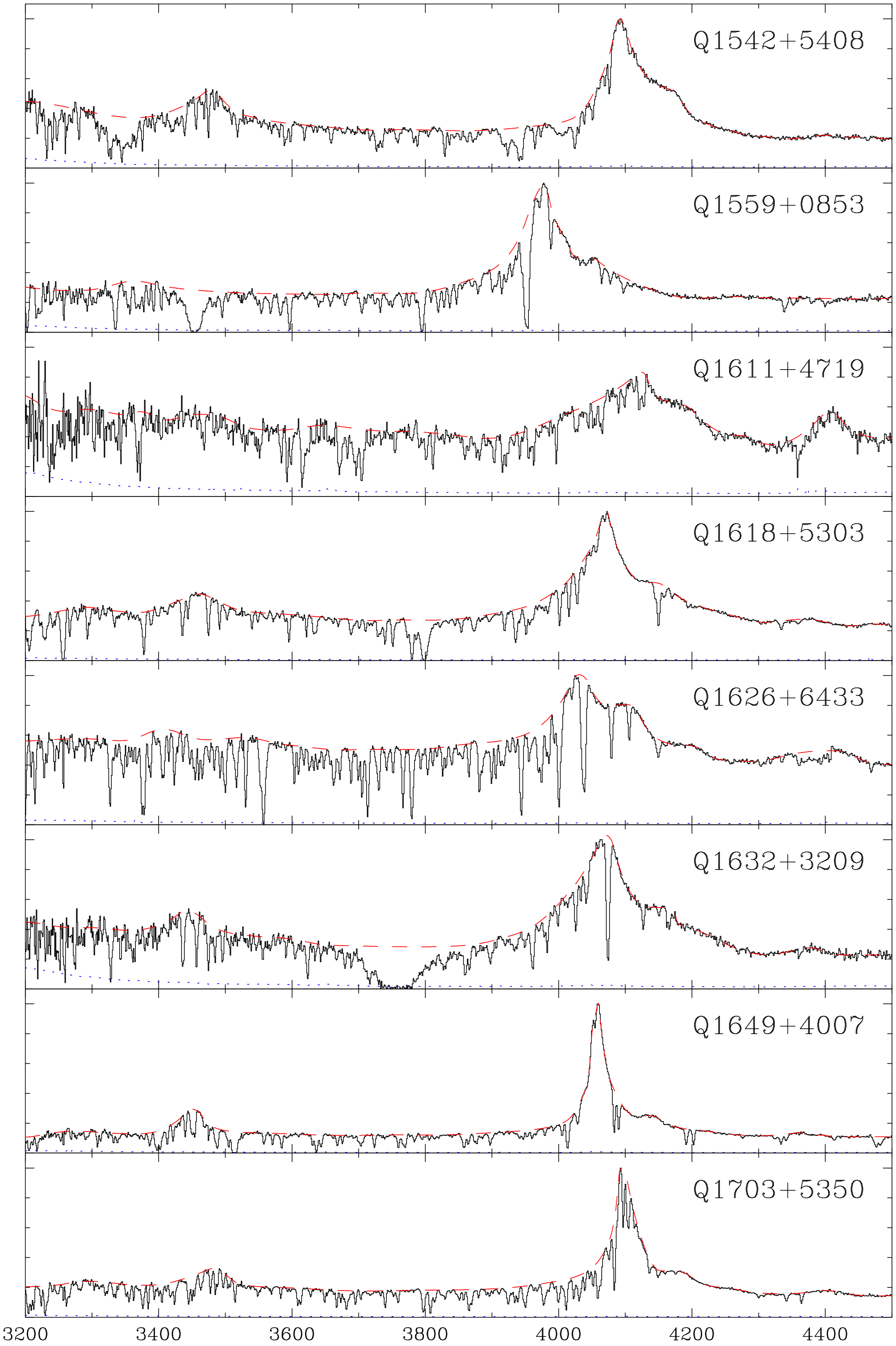

Fig. 14.— Same as for Figure 2.

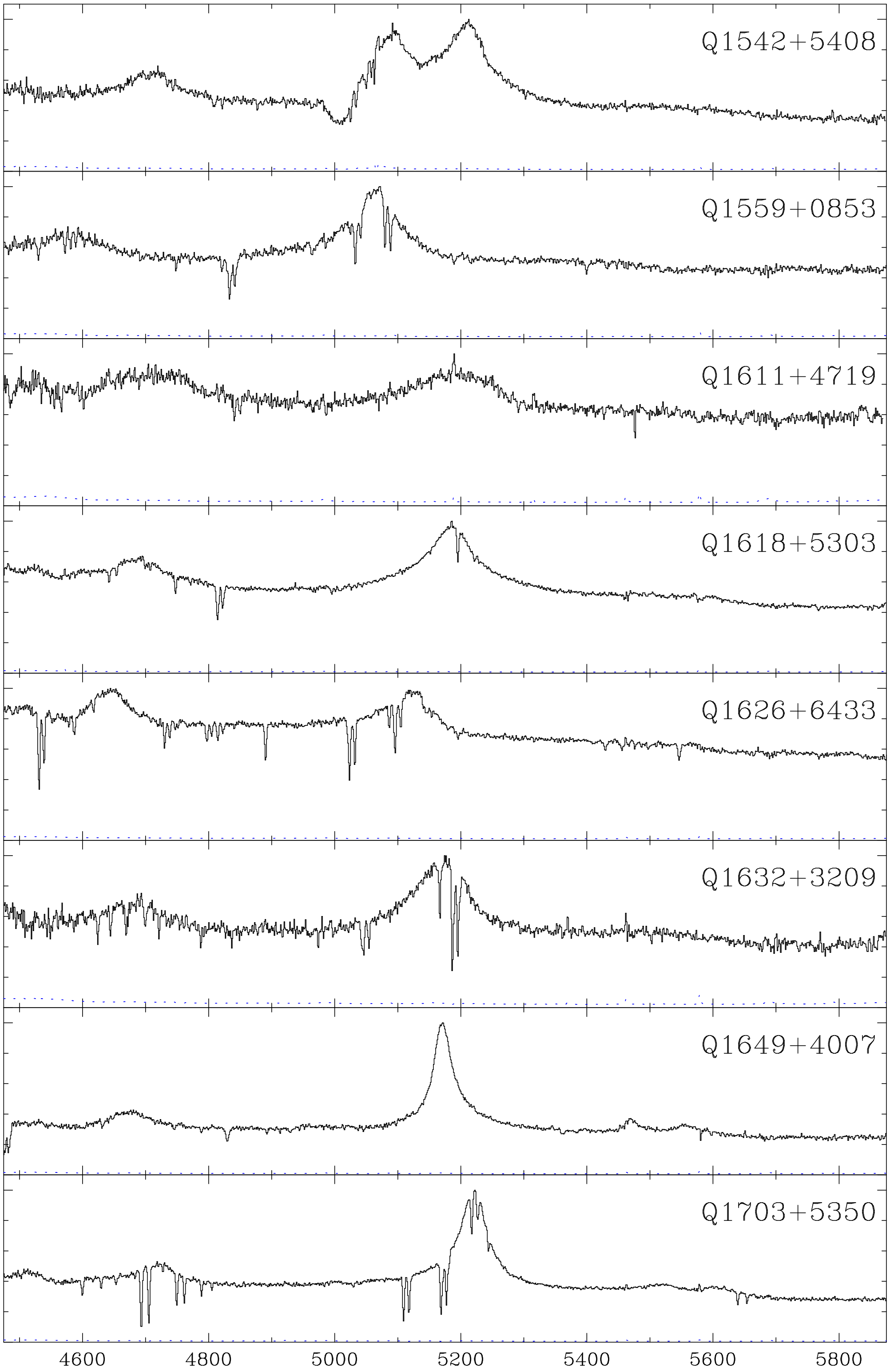

Fig. 15.— Same as for Figure 3.

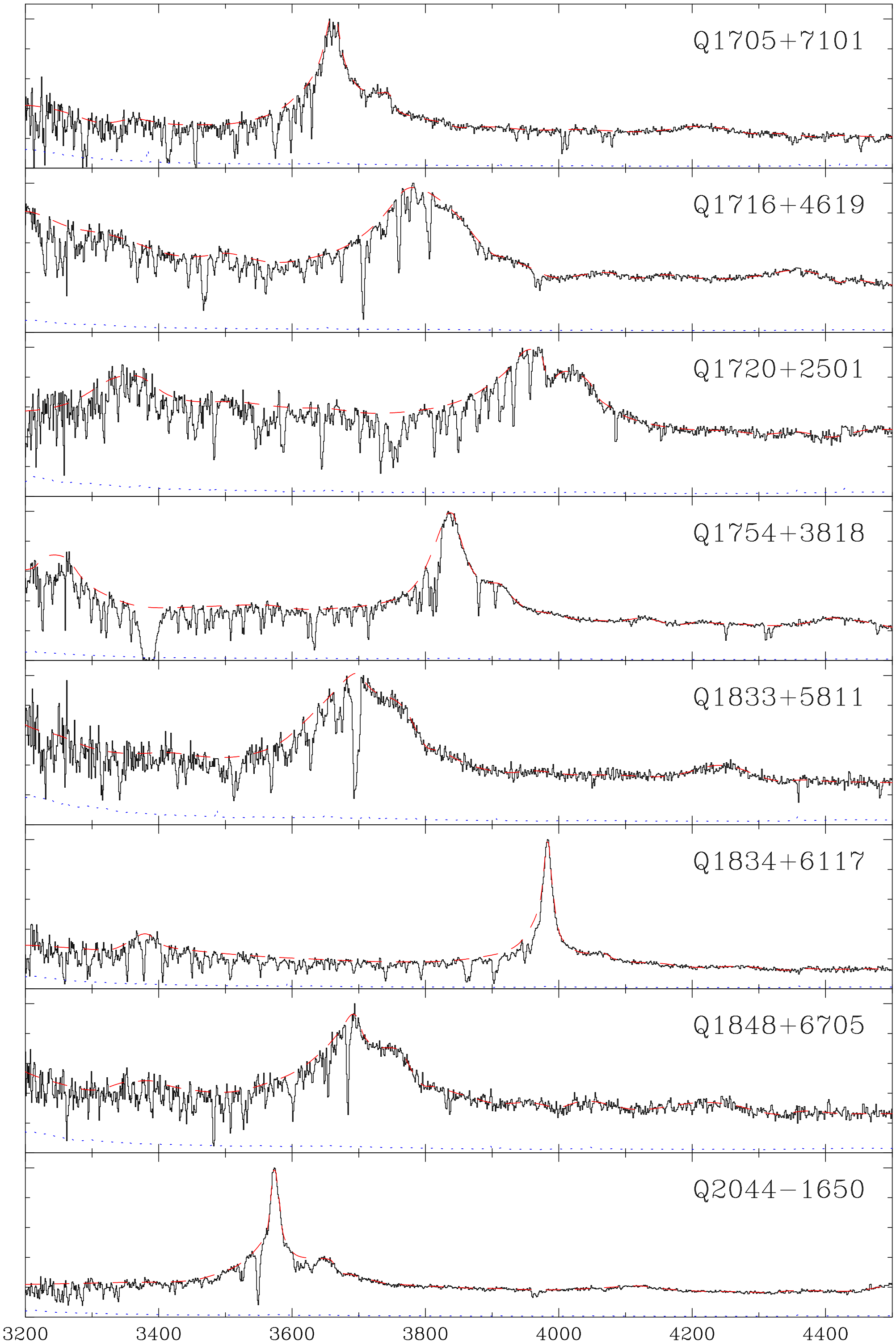

Fig. 16.— Same as for Figure 2.

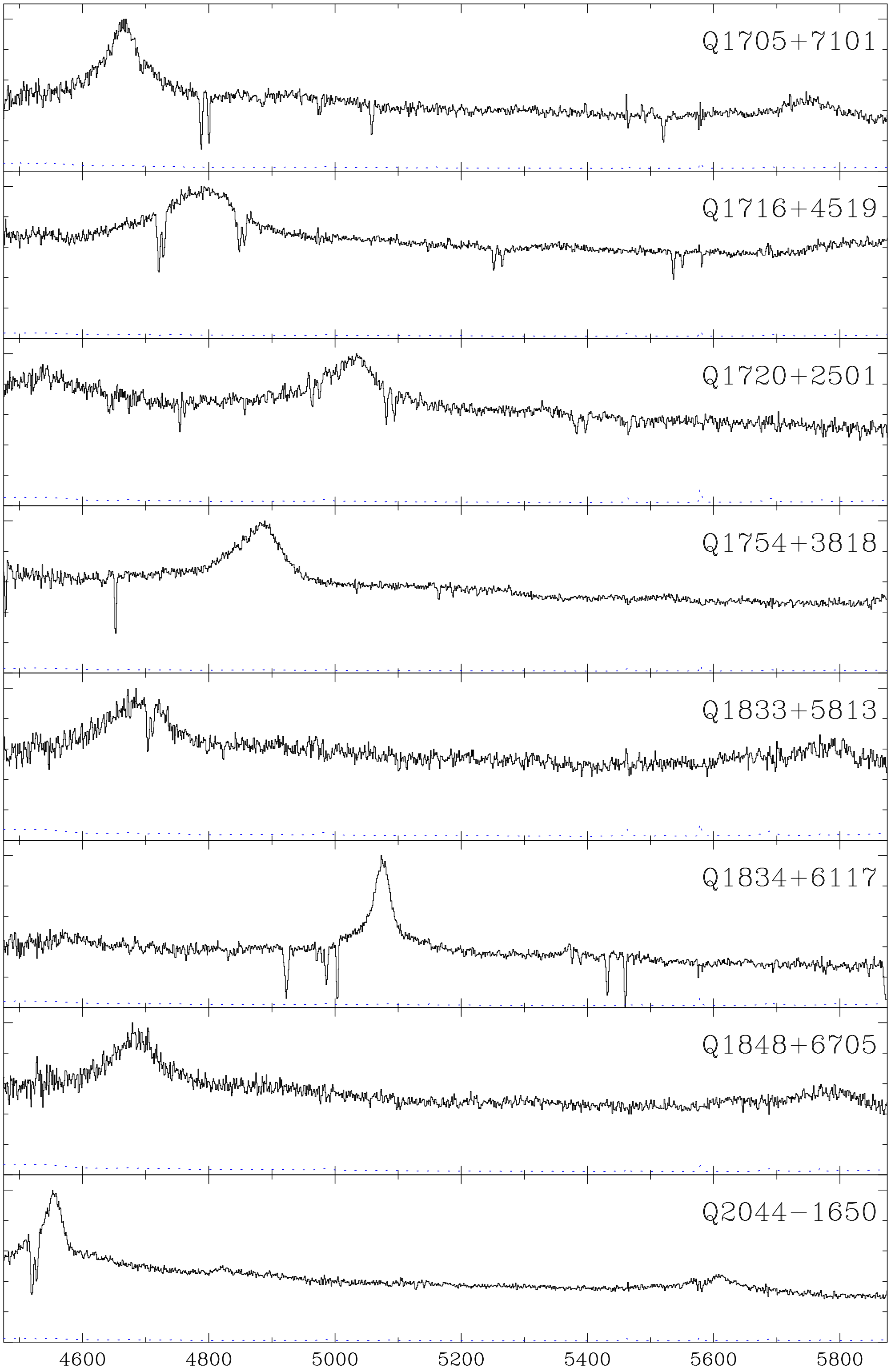

Fig. 17.— Same as for Figure 3.

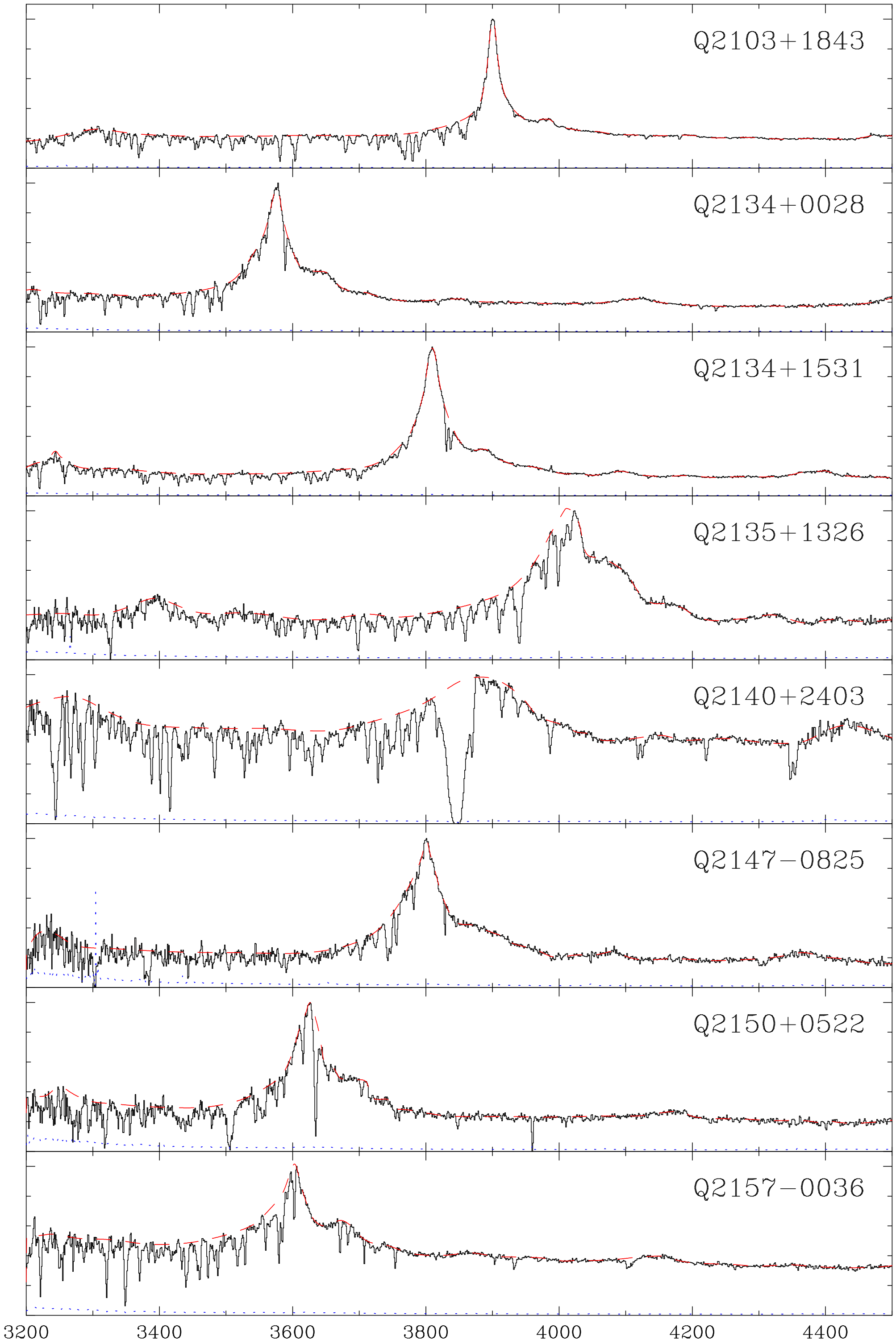

Fig. 18.— Same as for Figure 2.

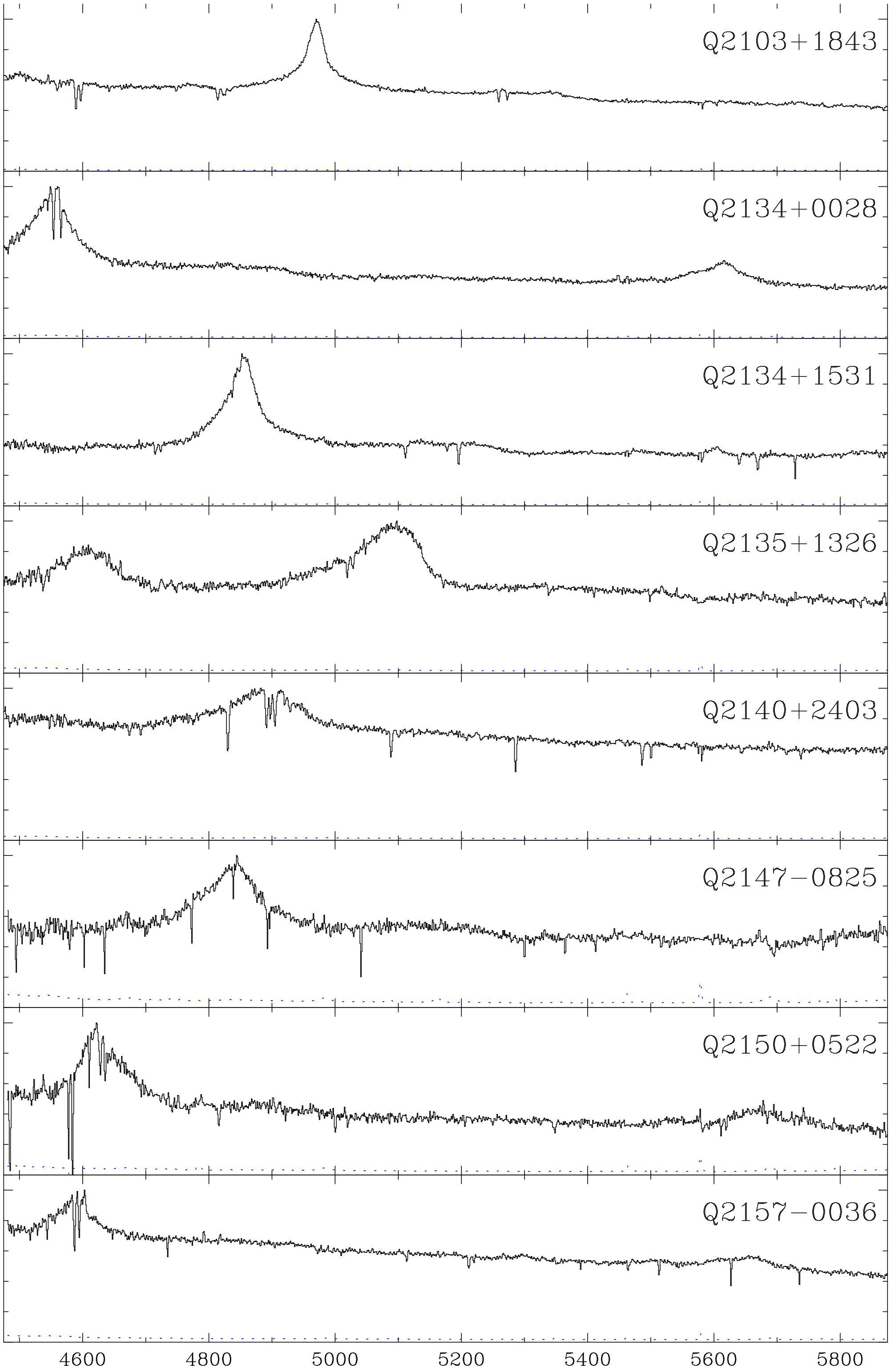

Fig. 19.— Same as for Figure 3.

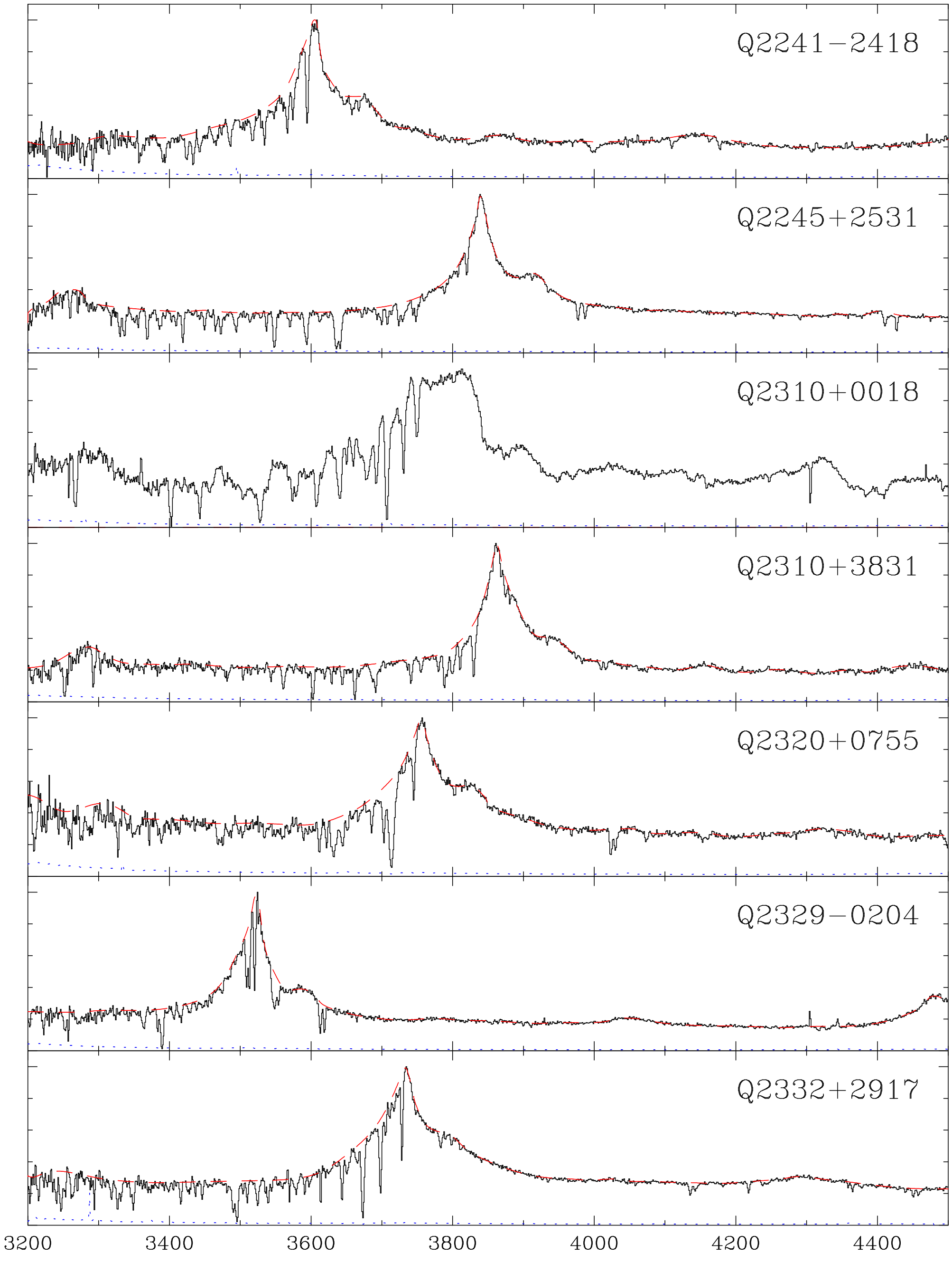

Fig. 20.— Same as for Figure 2.

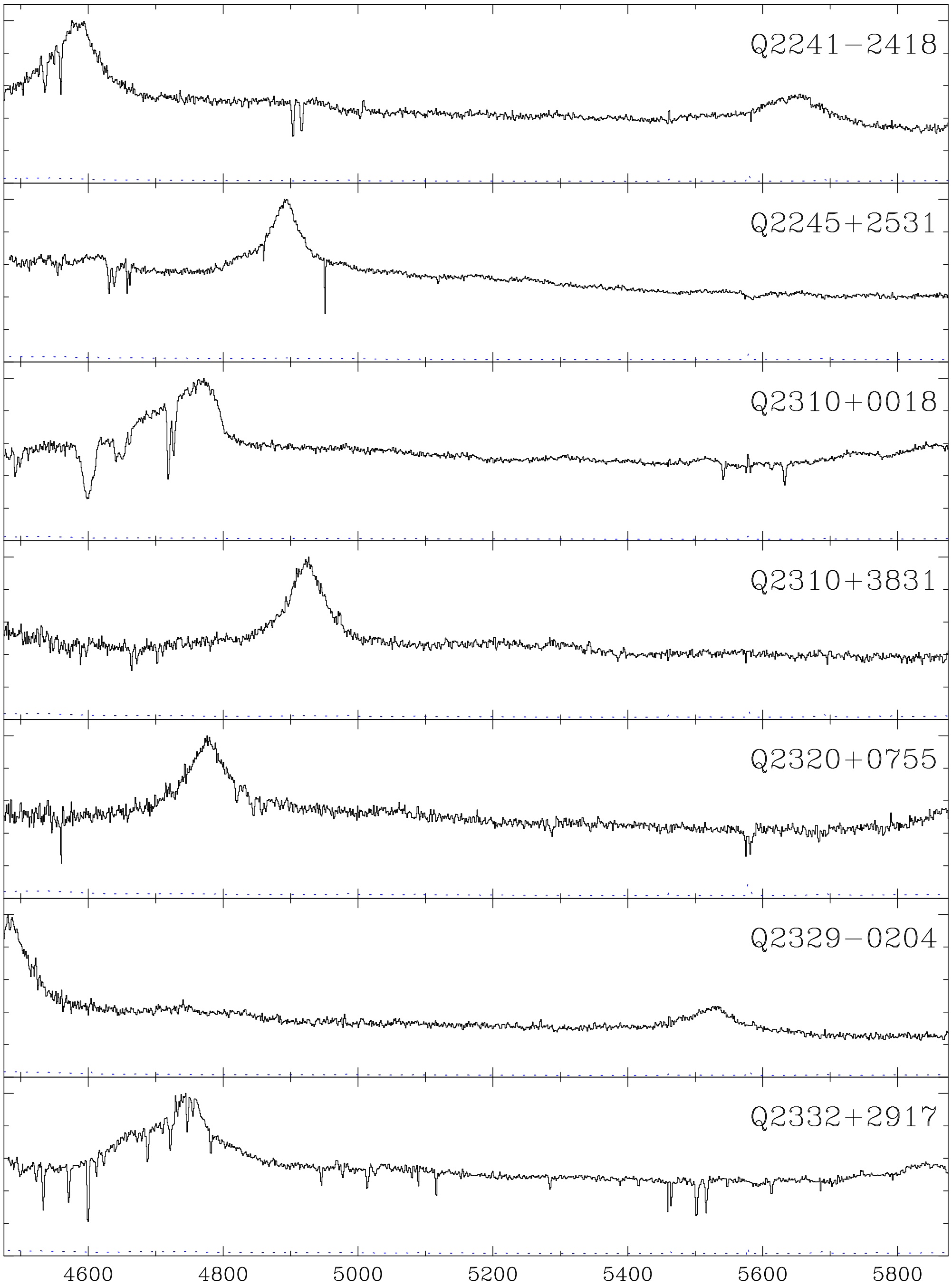

Fig. 21.— Same as for Figure 3.